

AD-A254 310



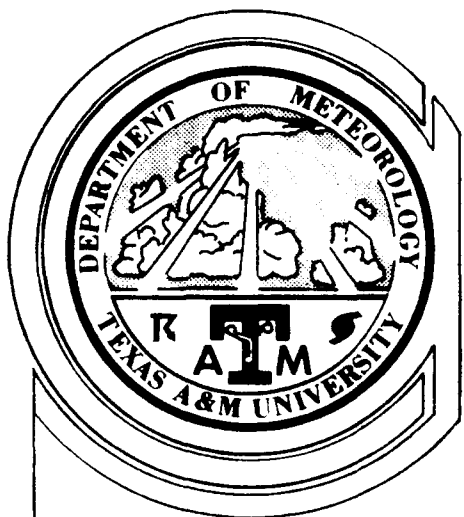
FORMATION PAGE

Form Approved
OMB No. 0704-0188

①

To average 1 hour per response, including the time for reviewing instructions, searching existing data sources, gathering the required information, and completing the collection of information. Send comments regarding this burden estimate or any other aspect of this collection of information, including suggestions for reducing this burden estimate, to Washington Headquarters Services, Directorate for Information Operations and Reports, 1215 Jefferson Davis Highway, Suite 1204, Arlington, VA 22202-4302, and to the Office of Management and Budget, Paperwork Reduction Project (0704-0188), Washington, DC 20503.

1. AGENCY USE ONLY (Leave blank)		2. REPORT DATE December 1991		3. REPORT TYPE AND DATES COVERED THESIS	
4. TITLE AND SUBTITLE Interactions of Tropical Synoptic-Scale Features as Viewed From Satellite				5. FUNDING NUMBERS	
6. AUTHOR(S) Susan E. Winton, Captain					
7. PERFORMING ORGANIZATION NAME(S) AND ADDRESS(ES) AFIT Student Attending: Texas A & M University				8. PERFORMING ORGANIZATION REPORT NUMBER AFIT/CI/CIA-92-065	
9. SPONSORING / MONITORING AGENCY NAME(S) AND ADDRESS(ES) AFIT/CI Wright-Patterson AFB OH 45433-6583				10. SPONSORING / MONITORING AGENCY REPORT NUMBER	
11. SUPPLEMENTARY NOTES					
12a. DISTRIBUTION / AVAILABILITY STATEMENT Approved for Public Release IAW 190-1 Distributed Unlimited ERNEST A. HAYGOOD, Captain, USAF Executive Officer				12b. DISTRIBUTION CODE	
13. ABSTRACT (Maximum 200 words) <div style="text-align: center;"> 92 8 24 009</div> <div style="text-align: right;"></div>					
14. SUBJECT TERMS				15. NUMBER OF PAGES 96	
				16. PRICE CODE	
17. SECURITY CLASSIFICATION OF REPORT	18. SECURITY CLASSIFICATION OF THIS PAGE	19. SECURITY CLASSIFICATION OF ABSTRACT	20. LIMITATION OF ABSTRACT		



TEXAS A&M UNIVERSITY

DEPARTMENT OF METEOROLOGY

INTERACTIONS OF TROPICAL SYNOPTIC-SCALE FEATURES AS VIEWED FROM SATELLITE

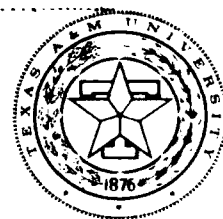
A Thesis

by

SUSAN ELIZABETH WINTON

Submitted to the Office of Graduate Studies of
Texas A&M University
in partial fulfillment of the requirements for the degree of
MASTER OF SCIENCE

December 1991



INTERACTIONS OF TROPICAL SYNOPTIC-SCALE
FEATURES AS VIEWED FROM SATELLITE

A Thesis

by

SUSAN ELIZABETH WINTON

Submitted to the Office of Graduate Studies of
Texas A&M University
in partial fulfillment of the requirements for the degree of
MASTER OF SCIENCE

DTIC QUALITY INSPECTED 2

December 1991

Accession For	
NTIS GRA&I	<input checked="checked" type="checkbox"/>
DTIC TAB	<input type="checkbox"/>
Unannounced	<input type="checkbox"/>
Justification	
By	
Distribution/	
Availability Codes	
Dist	Avail and/or Special
A-1	

Major Subject: Meteorology

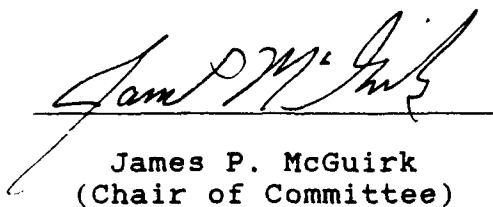
INTERACTIONS OF TROPICAL SYNOPTIC-SCALE
FEATURES AS VIEWED FROM SATELLITE

A Thesis

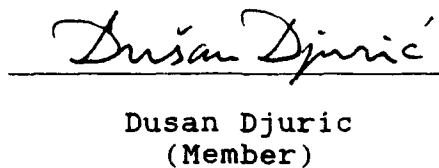
by

SUSAN ELIZABETH WINTON

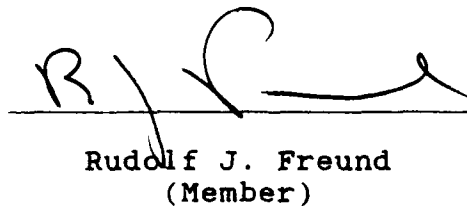
Approved as to style and content by:



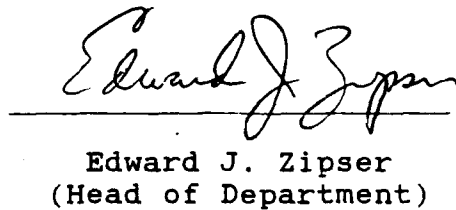
James P. McGuirk
(Chair of Committee)



Dusan Djuric
(Member)



Rudolf J. Freund
(Member)



Edward J. Zipser
(Head of Department)

December 1991

ABSTRACT

Interactions of Tropical Synoptic-Scale
Features as Viewed From Satellite. (December 1991)

Susan Elizabeth Winton, B.S., Gannon University

Chair of Advisory Committee: Dr. James P. McGuirk

Tropical synoptic features - a hypothesized periodic 12 d oscillation over Central America and a 2800 km eastward propagating wave over the eastern Pacific - are examined in OLR and TOVS satellite observations. Their interactions with each other, with tropical plumes and intraseasonal oscillations are found to be weak.

Time series analysis of the area-averaged (140° - 40° W and 35° N- 35° S) daily OLR for 1984 revealed a persistent 12 d oscillation in convective activity during dry (1 January - 9 May) and wet (10 May - 4 December) seasons. A spurious 7 d spike related to the amplitude of OLR values in convective regions, was removed. Composite diagrams of the phases of the oscillation (Maximum, Minimum and inflection points) revealed a preferred meridional orientation of OLR anomalies with eastward movement in the dry season and westward movement in the wet season.

Coherent 2800 km waves on the tropical upper troposphere, examined in HIRS-2 Channel 3 (14.5 micrometers)

brightness temperatures, were found to be a result of unrectified limb scanning effects. This spurious signal survived time averaging over multiple ascending and descending passes of two polar orbiters, climatological limb corrections by NESDIS, spatial interpolation and smoothing, and a tropopause height gradient that flipped the sign of the limb "darkening" effect. Nearly all the signal was removed by simple non-linear regression of the gridded data over both space and time. Findings by Schaefer (1988) and results of spatial filtering of OLR data suggest that a real wave of approximately 3000 km in length can exist and be masked by limb darkening.

Interactions between spatially filtered OLR data and tropical plumes were detected. Although some westward propagating convective maxima evolved into tropical plumes; many convective episodes, even those existing on 12 d time scales and 2800 km space scales, are not related to tropical plumes.

Possible connections between the 12 d oscillation and the 30-60 d oscillation were examined. The limited time series of this study prohibited firm conclusions being drawn, but obvious connections are absent.

ACKNOWLEDGMENTS

I acknowledge the members of my committee for their input and guidance. I especially want to express my thanks to the chair of my committee, Dr. James P. McGuirk, for his suggestions, encouragement, and non-linear support.

I thank the US Air Force for providing me with this opportunity to continue my education. Thanks also to my fellow graduate students in the department for your friendship and technical advice.

Finally, Joylyn, thank you for putting up with a mother who had to dedicate a lot of time to complete this study.

DEDICATION

To my daughter, Joylyn; my parents, Ernest and Elizabeth; and my brothers, Ernest and Gregory. Without your support and encouragement, this project would not have been possible.

TABLE OF CONTENTS

CHAPTER		PAGE
I	INTRODUCTION	1
II	PREVIOUS WORK.	3
III	DATA	8
IV	OBJECTIVES AND PROCEDURES.	13
V	DETERMINATION AND ANALYSIS OF A 12 D WAVE.	16
	Methods of Analysis	16
	OLR Composite Diagrams.	30
VI	ANALYSIS OF A 2800 KM THERMAL WAVE	46
	Methods of Analysis	46
	Non-linear Regression	65
VII	INTERACTIONS OF TROPICAL SYNOPTIC-SCALE FEATURES	75
VIII	SUMMARY AND DISCUSSION	87
	REFERENCES	91
	VITA	96

LIST OF TABLES

TABLE	PAGE
1. List of tropical plumes and their origins used in the tropical plume composite. After Schaefer (1988)	49
2. Dates and locations selected for quiescent composite. No tropical plumes were evident. After Schaefer (1988).	51
3. List of tropical plumes for March 1984. Provided by J. G. Lee (Texas A&M Univ.).	84

LIST OF FIGURES

FIGURE	PAGE
1. Domain of study covering 140°-40°W and 35°N-35°S.	9
2. Dry season (1 January - 9 May 1984) daily raw OLR deviations for the domain between 140°-40°W and 35°N-35°S	18
3. As in Fig. 2, except wet season (10 May - 4 December 1984).	19
4. Difference of raw OLR values for days 16 and 17 of dry season (1 January - 9 May 1984).	21
5. Dry season (1 January - 9 May 1984) periodogram analysis plot of amplitude vs. frequency.	24
6. As in Fig. 5, except wet season (10 May - 4 December 1984).	25
7. 12 d filtered OLR time series for dry season (1 January - 9 May 1984)	28
8. As in Fig. 7, except wet season (10 May - 4 December 1984).	29
9. Composite diagram of Maximum OLR days in dry season (1 January - 9 May 1984). Contoured values represent deviations from seasonal averages in units of 10^{-1} Wm^{-2}	32
10. As in Fig. 9, except Maximum-to-Minimum OLR days.	33
11. As in Fig. 9, except Minimum OLR days	34
12. As in Fig. 9, except Minimum-to-Maximum OLR days.	35
13. Composite diagram of Maximum OLR days in wet season (10 May - 4 December 1984). Contoured values represent deviations from seasonal averages in units of 10^{-1} Wm^{-2}	39
14. As in Fig. 13, except Maximum-to-Minimum OLR days.	40
15. As in Fig. 13, except Minimum OLR days	41
16. As in Fig. 13, except Minimum-to-Maximum OLR days.	42

LIST OF FIGURES (continued)

FIGURE	PAGE
17. Analyzed HIRS-2 channel 3 brightness temperatures for 11 February 1984. Temperatures are in Kelvins (K) and contour interval is 1 K	47
18. 28° longitude filtered channel 3 brightness temperatures for 1 January - 31 March 1984 centered at 1°N over 136°-44° W in units of Kelvins.	54
19. As in Fig. 18, except 5°N	55
20. As in Fig. 18, except 9°N	56
21. As in Fig. 18, except 15°N.	57
22. As in Fig. 18, except 19°N.	58
23. As in Fig. 18, except 25°N.	59
24. As in Fig. 18, except 33°N.	60
25. Results of non-linear regression on 28° longitude filtered channel 3 brightness temperatures for 1 January - 31 March 1984 centered at 1°N over 136°-44°W in units of Kelvins	67
26. As in Fig. 25, except 5°N	68
27. As in Fig. 25, except 9°N	69
28. As in Fig. 25, except 15°N.	70
29. As in Fig. 25, except 19°N.	71
30. As in Fig. 25, except 25°N.	72
31. As in Fig. 25, except 33°N.	73
32. Results of filtering daily-averaged OLR gridded data (1 January - 9 May 1984) to fit a 2800 km wave, centered at the equator over 135°-45°W in Wm^{-1}	76
33. As in Fig. 32, except 3°N.	77
34. As in Fig. 32, except 10°N	78
35. As in Fig. 32, except 13°N	79

LIST OF FIGURES (continued)

FIGURES	PAGE
36. As in Fig. 32, except 20°N	80
37. Results of filtering daily-averaged OLR gridded data (1 January - 4 December 1984) to fit a 2800 km wave, averaged and centered at 5°N-5°S over 135°-45°W in Wm^{-2}	85

CHAPTER I

INTRODUCTION

Within the past several years, two features have been identified and documented in the tropical atmosphere - a 12 d oscillation in Outgoing Longwave Radiation (OLR) over the Central American region and a 2800 km thermal wave over the tropical Pacific Ocean. This study aims to increase our knowledge of these features using statistical analysis techniques to document their mean behavior and to attempt to relate the synoptic-scale interactions of the two waves to each other and to other features of the tropical atmosphere.

The tropical atmosphere over oceans is a data sparse region. Satellites have been useful in providing remotely sensed tropical data. With the increased availability of tropical data, our awareness of tropical synoptic features is expanding. In this study, spectral analysis techniques are applied to time series of area-averaged OLR. Composite OLR diagrams are constructed to determine whether convection in one area of the domain affects convection in the entire domain. A non-linear recursive band-pass filter is applied

The style is that of the *Monthly Weather Review*.

to TIROS Operational Vertical Sounder (TOVS) Channel 3 brightness temperatures. Hovmoller diagrams are constructed to determine the existence, strength and location of a 2800 km upper tropospheric thermal wave.

Chapter II contains a review of previous work concerning tropical synoptic-scale features and their time scales. The objectives and general procedures of this research are detailed in Chapter III. The data sets used in this study are described in Chapter IV. Chapter V consists of the analysis and results inferred from the OLR data. The TOVS data analysis and results are described in Chapter VI. In Chapter VII, the interactions of these tropical synoptic-scale features and other tropical features described in the literature review are detailed. Finally, a summary and discussion are contained in Chapter VIII.

CHAPTER II

PREVIOUS WORK

Numerous studies on tropical synoptic-scale systems have revealed oscillations in atmospheric variables that range from three days to more than 60 d. See Riehl (1954), Atkinson (1971) or Hastenrath (1988) for a comprehensive review of these synoptic systems. Historically, the first identified synoptic feature were waves in the easterlies. These disturbances were recognized by Dunn (1940) in the Caribbean. Riehl (1945) states that these waves are a result of barotropic instability in the easterly current over Africa. These waves have zonal wavelengths between 3000 and 4500 km, propagate westward at an average speed of $5-8 \text{ ms}^{-1}$, and have a period of approximately 3-4 d. The top of the moist layer to the west of the trough axis can be as low as 1500 m. It rises rapidly near the trough axis reaching its maximum height of nearly 9000 m to the east of the axis. This deep moist area is normally associated with strong convective activity.

Merritt (1964) expanded on Riehl's work by including several variations of the easterly wave model. There has been a tendency to label any disturbance in the easterlies an easterly wave. Atkinson (1971) stated that many forecasters

used the easterly wave to explain all tropical weather occurrences. Riehl argued that tropical storm development was caused by an intensification of waves in the easterlies. An opposing view was held by Sadler (1967), who stated that all tropical vortices form initially in a shear zone existing between two opposing currents; this feature is commonly called a TUTT (tropical upper tropospheric trough). In spite of the controversies and regardless of what the weather systems are called, perturbations exist in the easterly flow that produce significant variations in convective activity in the tropics.

Atmospheric oscillations with periods longer than 10 d were discovered in the late 1960s. Wallace and Chang (1969) used spectral analysis techniques to identify oscillations in the horizontal wind components, relative humidity and surface pressure; these oscillations possess periods of 4-5 d. Also detected was a longer-period oscillation in these variables of greater than 10 d. This oscillation was strongest at the Western Pacific stations of their study. The authors downplayed this finding and attributed it to the sensitivity of the spectra at low-frequencies to minor changes in the sampling period. They wrote that a change in the period of study would have shifted or eliminated the spectral peak.

Madden and Julian (1971) presented the first real evidence of a tropical oscillation with a period greatly exceeding that of an easterly wave. Spectral analysis

techniques were applied to daily rawinsonde data for Canton Island (3°S , 172°W). They revealed a 41-53 d oscillation in the 85 and 15 kPa zonal wind, tropospheric temperature and station pressure over the tropical Central Pacific. To determine the spatial extent of this oscillation, Madden and Julian (1972) expanded their original study to include several tropical stations from around the globe. The results of the second study revealed an eastward-propagating, large-scale oscillation with a period of approximately 40-50 d. This oscillation was evident in station pressure and zonal wind for all stations within 10° latitude of the equator.

Satellite cloud cover and OLR data began to be used in the 1970s to detect low-frequency oscillations in the tropics. Yasunari (1980), using satellite cloud data and geopotential heights, found that the intra-seasonal variation of the Indian Monsoon during northern summer is dominated by the 40-50 d oscillation. Peaks of 15-30 d in OLR data over regions of southeast Asia during winter were identified by Murakami (1980). Lyons (1981) found similar spectral peaks over Indonesia and the equatorial Pacific regions. These studies demonstrate that convective activity in the tropics can be represented with OLR data - small OLR values indicate areas of high cloudiness (usually associated with convective activity) and large values indicate relatively cloud-free areas (at least above the trade wind layer). A series of papers followed which used OLR data to detect low-frequency

oscillations in the tropics: Lau and Lau (1990), Lau et al. (1989), Lau and Chan (1983), Liebmann and Hendon (1990), Weickmann (1983), Weickmann et al. (1985), and Knutson et al. (1986). Most of the previously mentioned studies were over the Indian Ocean and the western Pacific region. Some potentially significant OLR fluctuations were detected by Knutson and Weickmann (1987) over parts of Central and South America and also over the eastern Pacific Ocean. This tropical region has been largely ignored in the detection and significance of low-frequency oscillations. Strager (1989) used spectral analysis to identify a strong spectral peak at 12 d over Panama and portions of South America. Composite diagrams revealed an eastward propagating oscillation for the dry season of 1984 (1 January-9 May) that appeared to originate in the eastern Pacific and build to the east of Panama. The composites of the wet season (10 May-4 December) were remarkably different from those of the dry season in that the oscillation appeared to originate over Panama and drift to the west-northwest. This northwesterly movement has been detected also by Lau and Lau (1990).

The effectiveness of satellite data has been increased through the use of empirical orthogonal function (EOF) analysis. Smith and Woolf (1976) improved the accuracy of retrieved temperature profiles using EOFs. Anderson (1986) used EOF decomposition to retrieve synoptic scale signals from the satellite observed brightness temperatures.

Schaefer (1988) extended this work and employed a non-linear regression technique to analyze channel brightness temperatures from TOVS instruments on National Oceanic and Atmospheric Administration (NOAA) polar orbiters to locate and describe synoptic scale tropical waves. An apparently new observed feature of the tropical atmosphere was identified in this study. He documented a 2800 km tropospheric thermal wave which moved eastward in the upper troposphere (between 10 and 70 kPa) over the Eastern Pacific. Schaefer further linked this wave to the development of tropical plumes, as described by McGuirk et al. (1987).

In summary, satellites (particularly OLR and TOVS) have helped us to increase our knowledge of tropical synoptic systems. New synoptic scale features in the tropical atmosphere are being continually identified. Further research on the nature and structures of these features and their interaction is required. The focus of this research is the 12 d wave over Central America, the 2800 km thermal wave over the Eastern Pacific, and their potential interactions with each other and with some of the other atmospheric signals.

CHAPTER III

DATA

There are two main data sets used in this study. The first set is the NOAA Outgoing Longwave Radiation (OLR) data set. This data set, established in June 1974, is nearly continuous up to the present, and has been used in numerous studies of the tropics. The second data set consists of satellite-derived brightness temperatures observed by the TIROS Operational Vertical Sounder (TOVS) flown on the same NOAA polar orbiters; this set is archived at the National Environmental Satellite Data and Information Service and on the operational history tapes at the National Meteorological Center (NMC); it is used operationally to construct temperature soundings, but it can also be used diagnostically in raw forms, as well. The period of study for the OLR data set is divided into two distinct seasons - dry season (1 January-9 May 1984) and wet season (10 May-4 December 1984). The period of study for the TOVS data set is 1 January through 31 March 1991. The domain is 40°W - 140°W and 35°N - 35°S (Fig. 1). A brief description of each data set and collection process is provided here.

The NOAA OLR data were derived from window radiance measurements obtained from a scanning radiometer aboard the

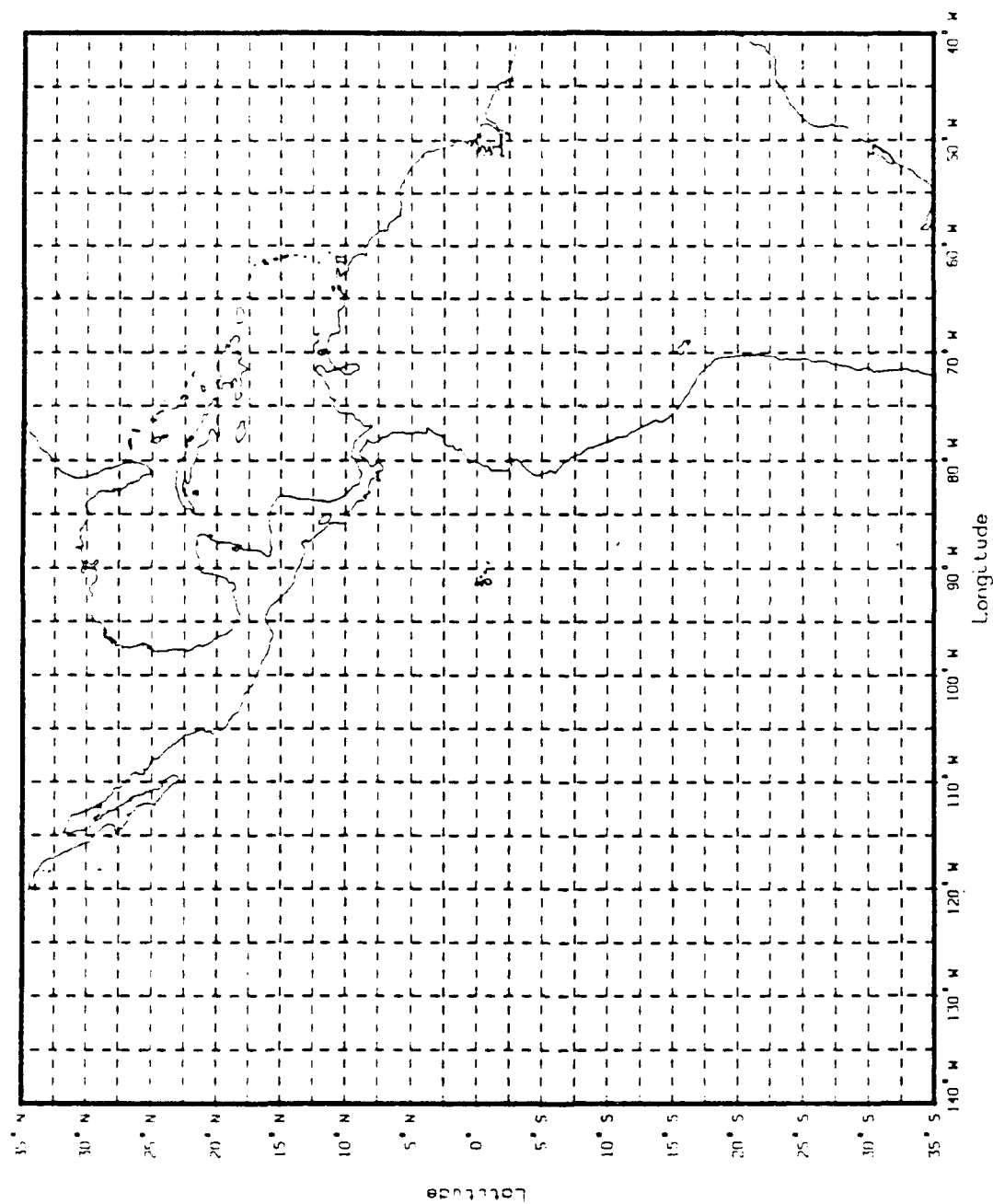


Figure 1. Domain of study covering 140°-40°W and 35°N-35°S.

NOAA-7 polar-orbiting satellite. The NOAA-7 is a sun-synchronous satellite and has equatorial crossing times of 0230 and 1430 LST. The original spatial resolution was 8 km but the observations have been spatially-averaged, digitized and stored in a 2.5° latitude-longitude array. This process is described by Gruber and Winston (1978).

Generally small values of OLR represent areas of deep convection and cloud cover, while large OLR values represent relatively cloud-free areas. OLR observations are one dimensional and do not provide any information on vertical structure, except approximate cloud top temperature.

The second data set consists of Channel 3 radiances obtained by TOVS flown on NOAA-7 and NOAA-8 operational polar orbiters. A detailed summary of the TIROS-N system (which is nearly identical to the NOAA-7 and NOAA-8 systems) is given by Smith et al. (1979). The TOVS is composed of three instruments: the High Resolution Infrared Radiation Sounder (HIRS-2, channels 1-20), the Microwave Sounding Unit (MSU, channels 21-24), and the Stratospheric Sounding Unit (SSU, channels 25-27).

Each channel measures the radiation within bands at certain wavelengths. The satellite-detected channel radiance can be used to infer a brightness temperature related to the temperature and atmospheric composition at different atmospheric levels by knowing something about the mean vertical distribution of atmospheric constituents. Channel 3 (at

14.50 micrometers) is sensitive to carbon dioxide and has its peak energy emission to the satellite near 10 kPa. Roughly speaking, it measures the vertical mean temperature in a 20 kPa deep layer centered approximately on the tropical tropopause.

The HIRS-2 instrument has a circular resolution of 30 km diameter at the sub-satellite point and the MSU resolution is 110 km at nadir. The resolutions decrease and the fields of view (FOV) become elliptical as the instrument scan moves away from nadir. The MSU measurements are interpolated to HIRS-2 scan positions to form a single set of radiances for each HIRS-2 location. The SSU radiances are processed separately and used to update a global latitude-longitude gridpoint analysis. From this analysis, they can be interpolated to the HIRS-2 locations. The radiance sets are combined into 63 FOV consisting of 9 scan spots across the satellite track and 7 scan spots along the track. Soundings are derived from these FOV ensembles with a resolution of approximately 250 km. A single set of radiances at 27 discrete bands results for each HIRS-2 spot.

Only HIRS-2 Channel 3 is used in this study, and retrieved soundings are not used. Schaefer (1988) found Channel 3 to be useful because the signal for this channel was located near the level of maximum response for the tropospheric thermal wave - that is, the 2800 km wave which he documented. Channel 3 has the added feature of being

reliable in most cloud contaminated soundings where most tropospheric channels are unusable, because its signal is generally initiated above cloud top.

CHAPTER IV

OBJECTIVES AND PROCEDURES

The major goal of this research is to increase our knowledge of synoptic-scale systems and their interactions over the east Pacific and western Caribbean, through the use of satellite observations. To accomplish this goal, the first objective is to define the horizontal structure of convective variability associated with the 12 d oscillation (Strager, 1989) over the entire east Pacific/Central American basin. The second objective is to quantify a short climatology of the 2800 km thermal wave (Schaefer, 1988) over the same tropical area. Finally, this research will identify and relate any detectable synoptic-scale interaction between these two waves (if they exist) and between other tropical features. The only features that can be detected in OLR (clouds) or in tropopause level thermal variations are features such as horizontal and vertical distribution of cloud fields. Although more features are desirable, observations are not available to support a more comprehensive study.

These objectives are accomplished by completing approximately seven well defined analysis tasks.

Tasks required to accomplish the first objective are:

1. Preprocess NOAA OLR data for the dry season (1 January-9 May 84) and wet season (10 May-4 December 84) defined in prior research. Define regional indices, quality control data to remove trends, missing swathes, erroneous data, and compute basic descriptive statistics.

2. Identify the 12 d oscillation in the pre-processed OLR time series using spectral analysis and temporal filtering, and quantify domain mean behavior for this oscillation.

3. Construct composite OLR anomaly diagrams corresponding to the phases of the oscillation cycle, using both the OLR area averaged time series and OLR point time series.

Tasks required to accomplish the second objective are:

4. Preprocess NOAA-7 and NOAA-8 TOVS channel brightness temperatures for the same domain and the time period (1 January-31 March 1984). The processing will include: analyzing randomly located observations within specified synoptic time periods to grids similar to OLR observations; screening for errors in the observations; and interpolating for residual cloud contamination.

5. Identify the 2800 km wave feature and isolate it using non-linear regression techniques or non-linear filtering.

6. Quantify the behavior of the 2800 km wave as a

synoptic-scale tropical feature using non-linear regression techniques.

Task required to accomplish the third objective are:

7. Identify interactions between the 12 d wave with tropical plumes and the 30-60 d wave, if any interactions exist.

CHAPTER V

DETERMINATION AND ANALYSIS OF A 12 D WAVE

Strager (1989) concentrated his analysis to the behavior of the 12 d wave only over Panama (75° - 85° W, 5° - 12° N). He questioned the extent of this oscillation hypothesizing that its effects did not extend very far to the west over the Pacific Ocean and to the east over the Caribbean. The present study was initiated to determine the range of the 12 d wave and its structure and evolution over a much larger domain of the Western Hemisphere. The analysis methods employed herein closely follow those used by Strager (1989). The present analysis yielded results that required much more care in removing spurious coherent behavior in the gridded data fields.

Methods of Analysis

The OLR data were divided into the two distinct seasons: a dry season (1 January-9 May 1984) and a wet season (10 May-4 December 1984). This division was made to correspond with the divisions described by Strager (1989), and was necessary because of the differing convective behavior between the two seasons.

Two sets of averaged OLR values were calculated for the domain (140° - 40° W, 35° N- 35° S), using both the 0230 and 1430 LST gridded analysis. One set consisted of the average of the twice daily OLR observations to eliminate any variance resulting from the diurnal cycle. The second set consisted of area-averaged daily OLR values.

There are 1189 OLR grid points contained in the domain. A single daily mean OLR value was calculated for the domain by taking the average of the 1189 0230 LST and the 1189 1430 LST OLR point values. The area-averaging of the OLR greatly reduces the synoptic- and subsynoptic-scale signal and noise in the OLR time series, allowing an easy differentiation between local and large-scale events. Local fluctuations which appear as minor peaks in time series, may be random behavior not representative of climatological series or a larger domain. These area-averaged daily OLR values comprise the OLR time series for the domain and are used in the time series analysis. Time series of daily OLR averages for the dry season and wet season are shown in Figs. 2 and 3. The two series are of different lengths so the apparent differences in temporal behavior are misleading. In Fig. 2, the temporal and spatial mean of 234.7 Wm^{-2} has been removed from the area-averaged daily OLR values. Deviations from this mean range between -0.8 to $+1.4 \text{ Wm}^{-2}$; these anomalies represent OLR fluctuations averaged over approximately 10^8 km^2 . There is an indication of an oscillation of approximately 50

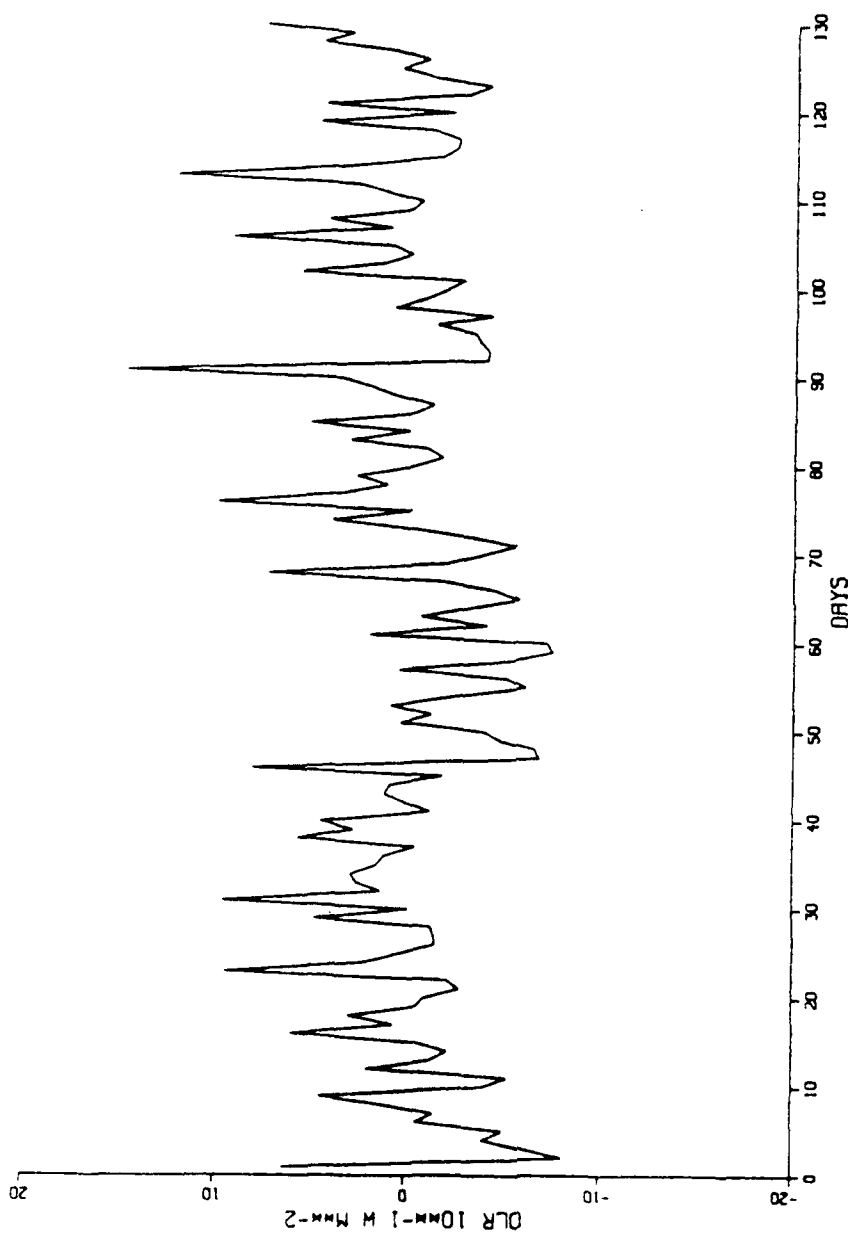


Figure 2. Dry season (1 January - 9 May 1984) daily raw OLR deviations for the domain between 140°-40°W and 35°N-35°S.

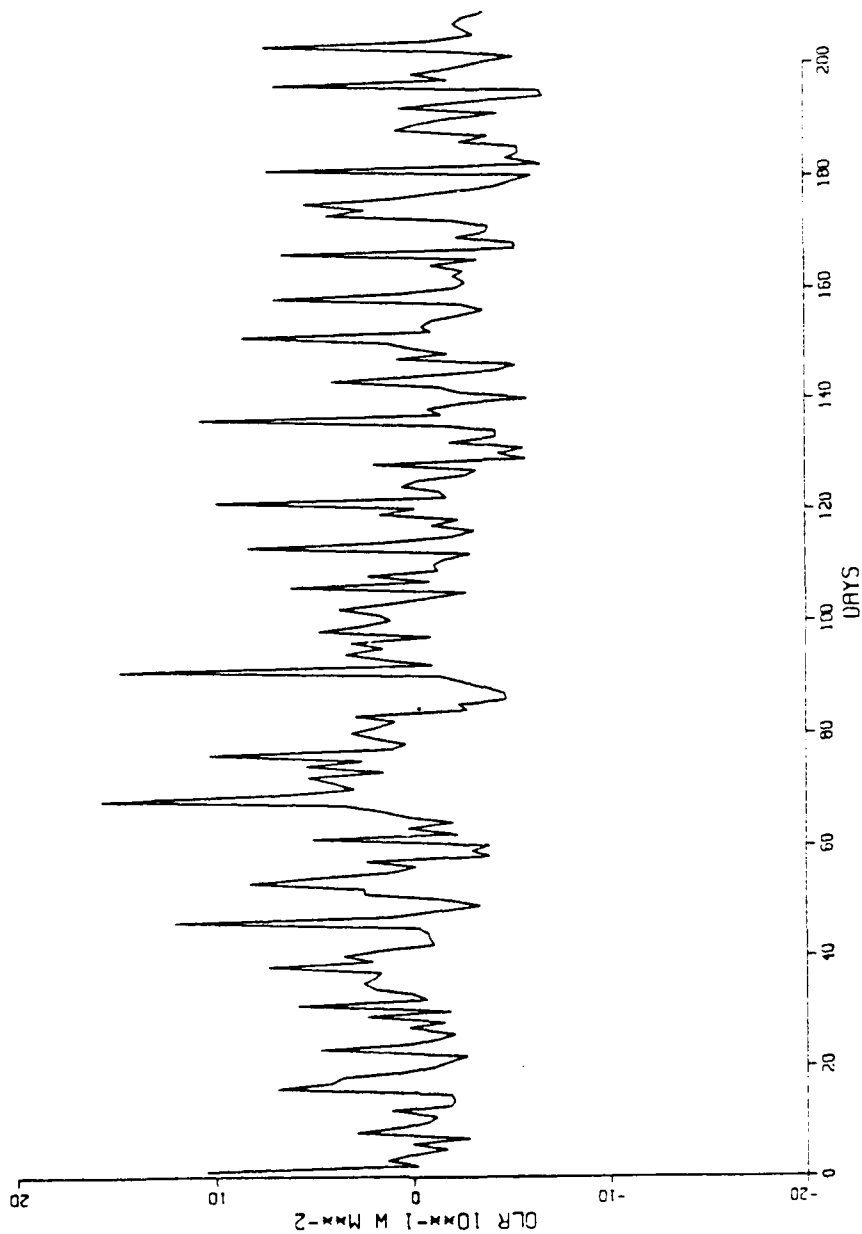


Figure 3. As in Fig. 2, except wet season (10 May - 4 December 1984).

d. Relative peaks are observed near day 30, day 85 and day 120. The mean of 235.7 Wm^{-2} was removed from the area-averaged daily OLR values in Fig. 3. The deviations from the mean range from -0.8 to $+1.5 \text{ Wm}^{-2}$. The oscillation near 50 d is not readily apparent although Knutson and Weickmann (1987) suggest that peaks near 60 d should be anticipated. This result is surprising because the 30-60 d wave is normally much stronger in the warm season.

An obvious spike every 7 d is apparent in both series and is more pronounced than the weak spike detected, but not discussed, by Strager (1989). This feature is a spike occurring approximately every seventh day; and is not simply an oscillation of 7 d periodicity. Because of this unusual behavior, it was anticipated that the feature is spurious. One can easily imagine an operational function or error occurring once a week, on a specified day, causing such a behavior. An examination of the raw OLR data (Fig. 4) showed the 7 d oscillation to be a recurring phenomenon located largely outside the area studied by Strager (1989). To examine the nature of this spike, and the structure of its spatial patterns, the OLR field for the day following the spike was subtracted from the day of the spike, for each spike throughout the time series. In Fig. 4, a typical difference of the raw OLR values, for days 17 and 16 of dry season, are plotted; day 16 spiked approximately 5 Wm^{-2} higher than day 17. This spike is actually small compared to

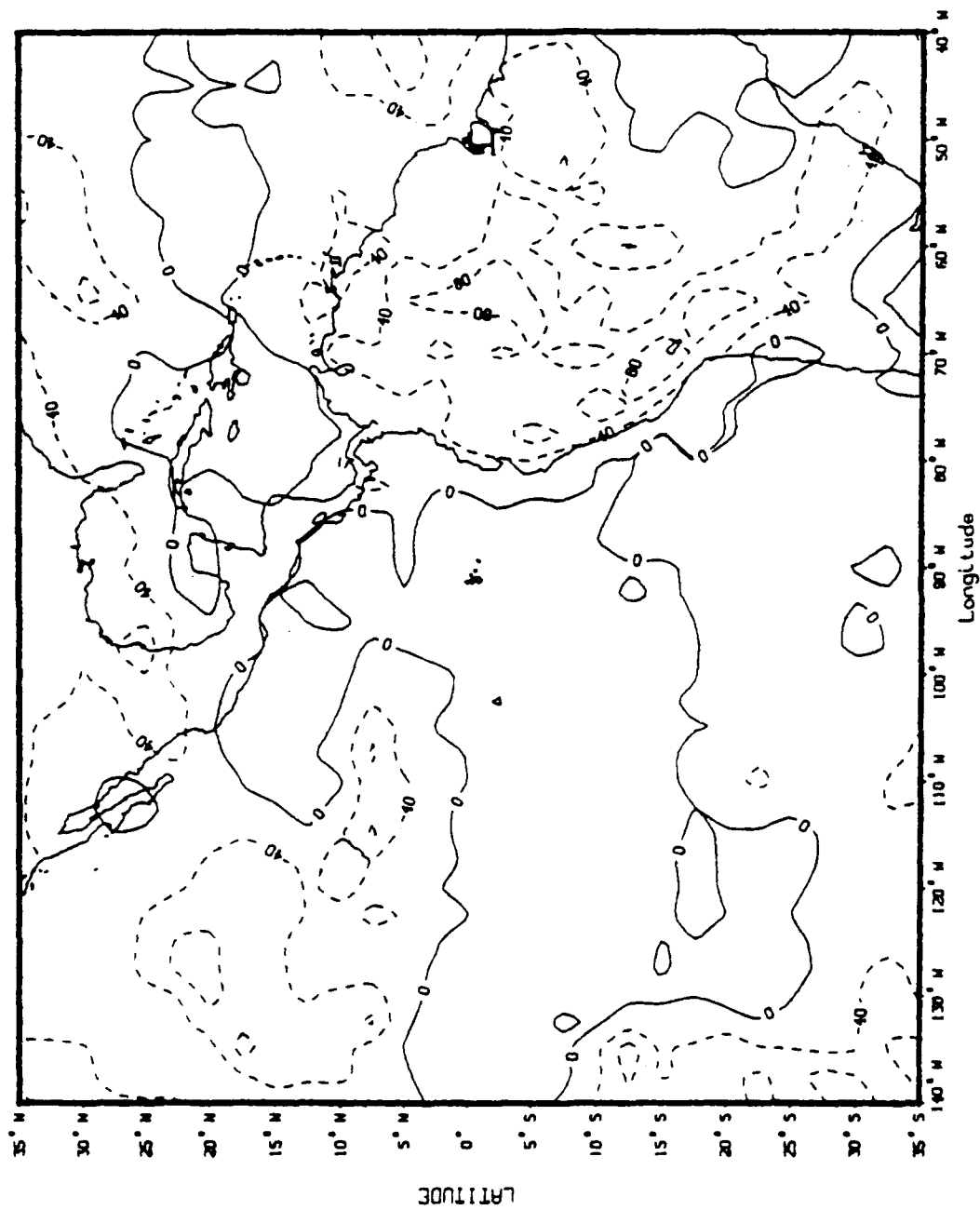


Figure 4. Difference of raw OLR values for days 16 and 17 of dry season (1 January - 9 May 1984).

many of the other observed spikes in Figs. 2 and 3, particularly in the wet season. Preferred locations for negative anomalies appear over South America and both the northeast and southeast subtropical Pacific basins. Given the weak amplitude of the spatial pattern of the spike over Central America, it is not surprising that the phenomenon was not noticed or deemed relevant by Strager (1989). This preference was noted in difference plots (not given here) for other peak days in both dry and wet seasons. The curious feature of the anomalies of the difference pairs is that the positive anomalies are almost non-existent. The 7 d pairs have almost no difference in the "equatorial" dry zone along the equator from the American coast into the Central Pacific. In the convective regions, most dominant over South America and to a lesser extent over the United States and central Pacific tropical region, the anomalies are large, sometimes as great as 10 Wm^{-1} . Differences in maps of the day before and the day after spikes (for example, days 16 and 18) show only typical expected synoptic scale differences. The precise cause of the spike is uncertain. It is marked, however, by systematically warmer OLR values in the convective regions. Two possibilities are: 1) The calibration of the coldest OLR observations are set too high for one day of the week. 2) Less likely, climatological fields are accidentally inserted one day a week. It is most unlikely that this behavior is real.

Time Series Analysis

Harmonic analysis, the process of decomposing a time record into the sum of sinusoids of various frequencies and amplitudes, is used to identify any significant periodicities in the OLR time series. The purpose behind harmonic analysis is to understand a complicated time series by breaking it up into these frequencies representing fundamental processes. Panofsky and Brier (1968) provide a detailed discussion of harmonic analysis. The type of harmonic analysis used in this study is the fast Fourier transform (FFT) method. The FFT method is described in the International Mathematical and Statistical Library User's Manual (IMSL, 1987). A computer routine that uses the FFT method to perform a periodogram analysis is provided in the IMSL User's Manual. This periodogram analysis calculates the sum of the squared amplitudes of the sinusoids, or spectral density, for each frequency. The IMSL periodogram analysis was done for the area-averaged daily OLR time series of each season, with the results shown in Figs. 5 and 6.

The two spectra possess only a weak red noise character throughout these time scales. The spectral behavior at time scales greater than about 20 d periodicities are based on only a few periods and may not be representative of longer time series. As seen in Fig. 5, the dry season shows a large spectral peak at around 52 d, with lesser peaks at around

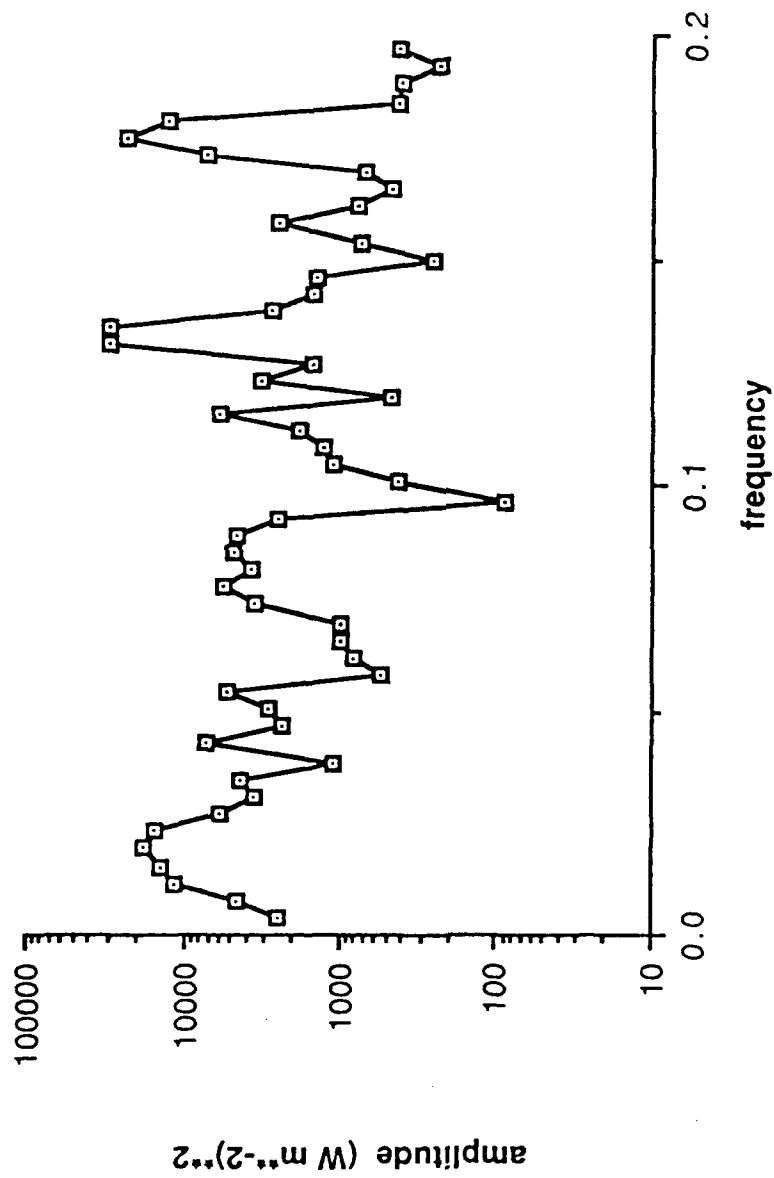


Figure 5. Dry season (1 January - 9 May 1984) periodogram analysis plot of amplitude vs. frequency.

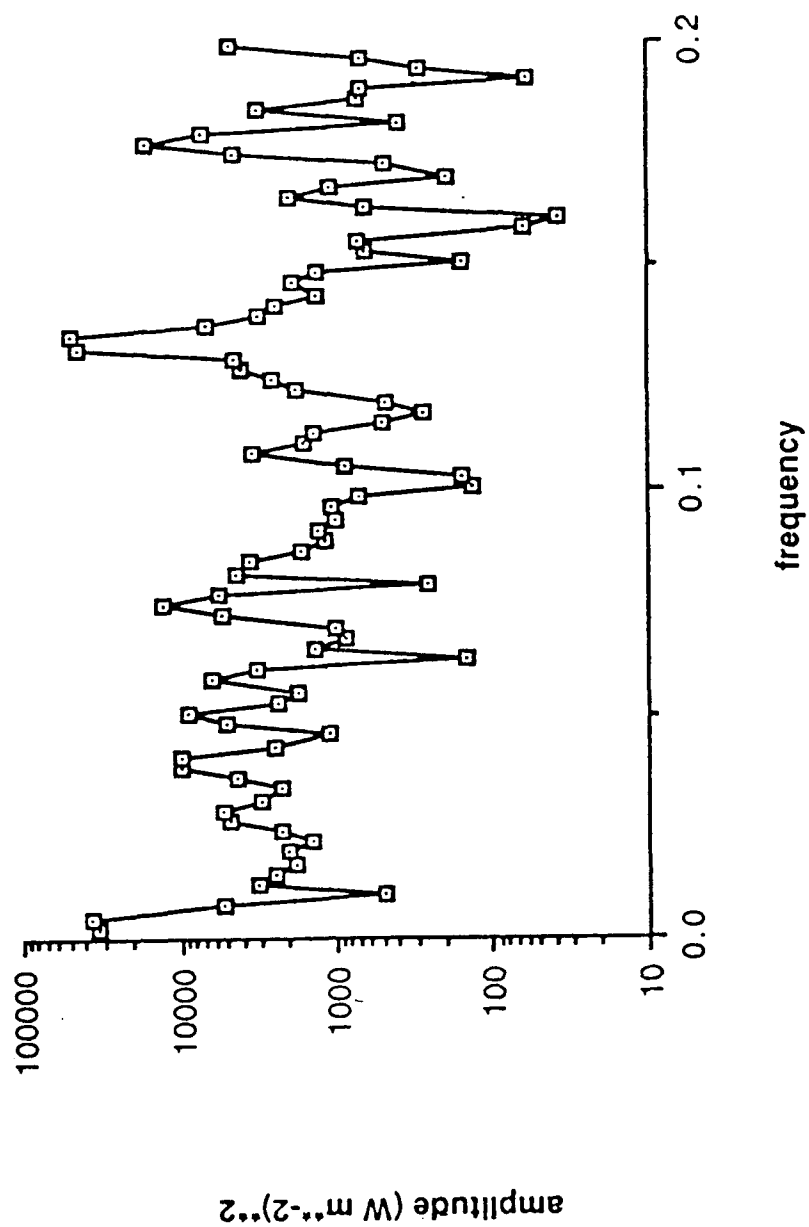


Figure 6. As in Fig. 5, except wet season (10 May - 4 December 1984).

24 d (0.04) and 13 d (0.08). The largest spectral peaks can be found at around 7 d and 5 d. As noted above, the peak at 7 d is not physically meaningful. The peak at 5 d has been previously observed in past OLR studies, but is not discussed here. In contrast, the periodogram analysis of dry season 1984 in Strager's study (1989, Fig. 13) shows a spectral peak at around 65 d with the largest spectral peak concentrated in the 11-12 d range. The wet season periodogram analysis in Fig. 6 shows spectral peaks at around the same days as in the dry season analysis, except the peak near 50 d is absent as anticipated from inspection of Fig. 3. The absence of this peak is inconsistent with the expectations based on results of Knutson and Weickmann (1987) who show significant amplitude fluctuations on this time scale in Hovmöller diagrams of OLR. Strager's (1989) wet season 1984 periodogram analysis (Fig. 14, in his study) showed a spectral peak of approximately 35-40 d with another high concentration of spectral density at around 12 d.

The periodogram analysis performed by Strager (1989) over the Panama region showed the strongest spectral peak to be located at around 12 d. In comparison, the periodogram analyses of the domain in this study reveals a weaker spectral peak at that time; it is reiterated that the spatial domains of the two studies are different.

To examine the temporal variation and steadiness of this 12 d oscillation, a non-linear recursive band-pass filter,

developed by Shanks (1967) and used by Murakami (1980) and Strager (1989), was applied to the OLR time series of Figs. 2 and 3. Each output point of the filtered series is computed as the weighted sum of input points plus a weighted sum of previously computed output points by this filter. The central frequency and half power amplitudes are set by the user of the filter. The periods chosen in this study were 12 d for full response, and 9 d and 15 d for 0.5 amplitude response to correspond with previous work done by Strager (1989).

The plots of the 12 d filtered OLR time series for both seasons are shown in Figs. 7 and 8. An examination of these diagrams shows that the 12 d oscillation is present in each season, although it is often larger in amplitude during the wet season and the dry season is slightly steadier. The salient feature of the filtered series is the steadiness of the oscillation. The daily standard deviation of the area-averaged time series is 1.2 Wm^{-2} (dry season) and 1.1 Wm^{-2} (wet season) so the peak-to-peak amplitudes are 50% of the mean temporal standard deviation. The amplitude varies from period to period. The period modulates slightly. But the oscillation is a continuous feature throughout both records. The character of the filtered series is dissimilar to that of filtered random series. Another item of interest in the wet season filtered time series is the apparent modulation of the

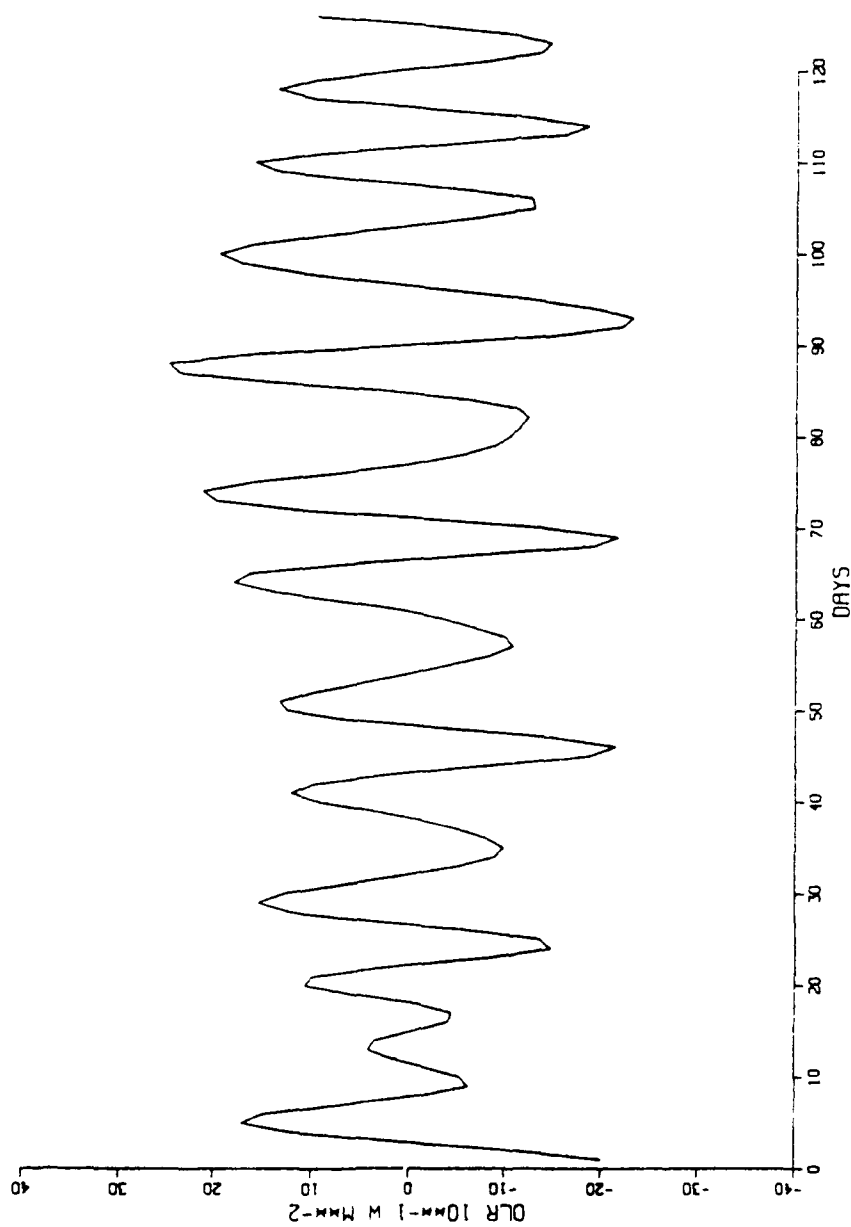


Figure 7. 12 d filtered OLR time series for dry season (1 January - 9 May 1984).

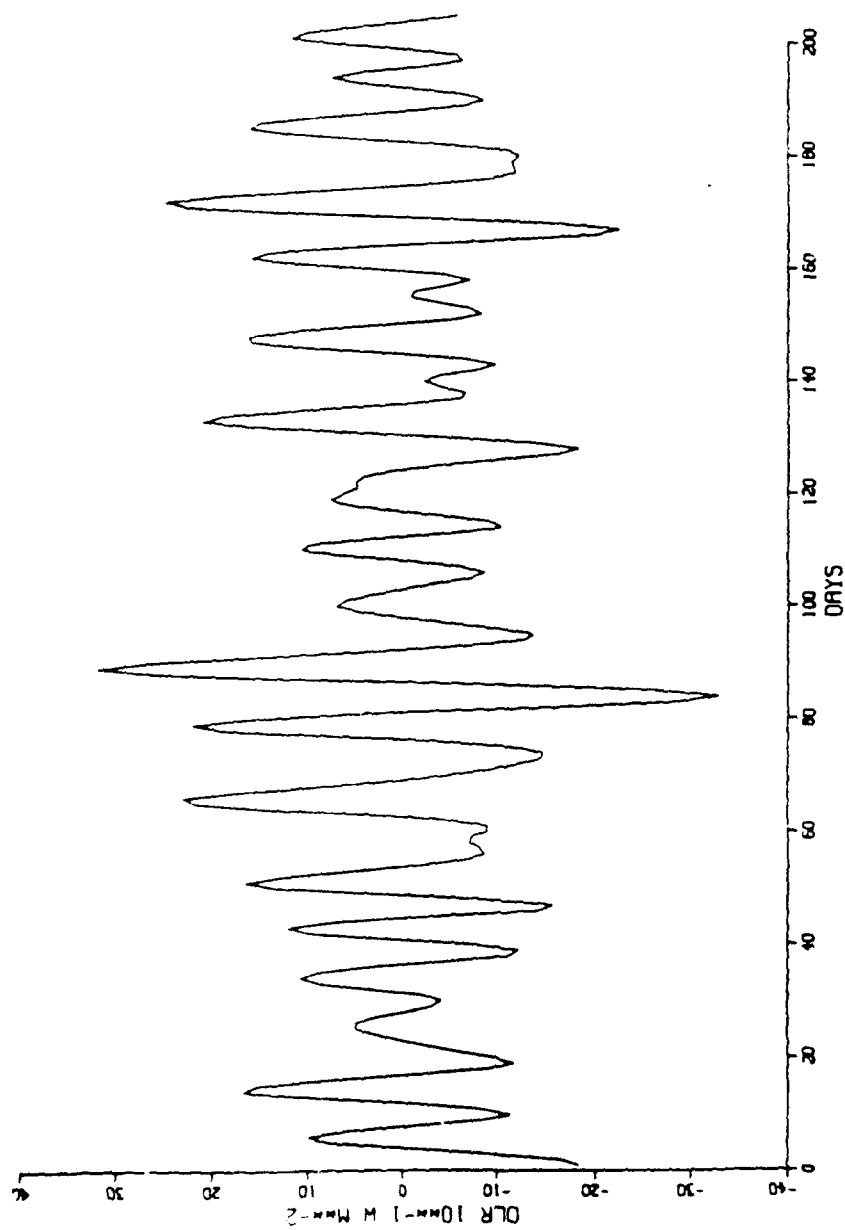


Figure 8. As in Fig. 7, except wet season (10 May - 4 December 1984).

12 d oscillation occurring every 70-80 d. This feature was also apparent in Strager's study (1989).

OLR Composite Diagrams

To determine the spatial pattern and range of the 12 d oscillation in the domain of this present study, OLR composite diagrams were constructed as follows:

- The OLR time series for each point throughout the domain was filtered for periods around 12 d in the same manner as the area-averaged time series in Figs. 7 and 8. This was done without first performing a spectral analysis to determine if any spectral peaks existed in that period at each point. The reasoning behind this procedure is that if no 12 d signal existed in any subregion of the domain, application of a 12 d filter to the OLR time series at each point would filter out all of the signal, resulting in time series that would show little or no OLR deviations.

- For each season, each day for which the area-averaged and filtered OLR attained a maximum value (a relatively cloud-free day) was selected and labelled a "Maximum OLR day". The 12 d filtered OLR values for each Maximum OLR day were collected and averaged for each point in the domain. The resulting spatial pattern formed the Maximum OLR days composite. The same procedure was used to construct a composite diagram corresponding to Minimum OLR days.

- Composite diagrams were also constructed for the two inflection points between OLR extrema found in the area-averaged and 12-d filtered time series. They correspond to the inflection point going from relatively cloud-free to cloudier conditions (Maximum-to-Minimum OLR) and going from cloudier to relatively cloud-free conditions (Minimum-to-Maximum OLR).

Composite Diagrams for Dry Season

The composite diagrams for the dry season are shown in Figs. 9, 10, 11 and 12. Each composite represents an average over 9 or 10 d. Arbitrarily beginning the 12 d cycle with the Maximum OLR composite (Fig. 9), a large area of maximum OLR deviations can be seen over most of the southern United States, Central America, and the western part of South America. Another band of positive anomalies extend along 45°W . Typical amplitudes vary between 3 and 10 Wm^{-1} . Large negative anomalies cover most of the east Pacific and extend north south between 45° and 65°W .

Three days later, the Maximum-to-Minimum inflection point composite (Fig. 10) shows a lessening in the strength of the positive OLR anomalies and areas in North America and Central America. The positive anomalies previously located in the southwestern corner of the domain have increased in area covering almost the entire Pacific Ocean in the Southern

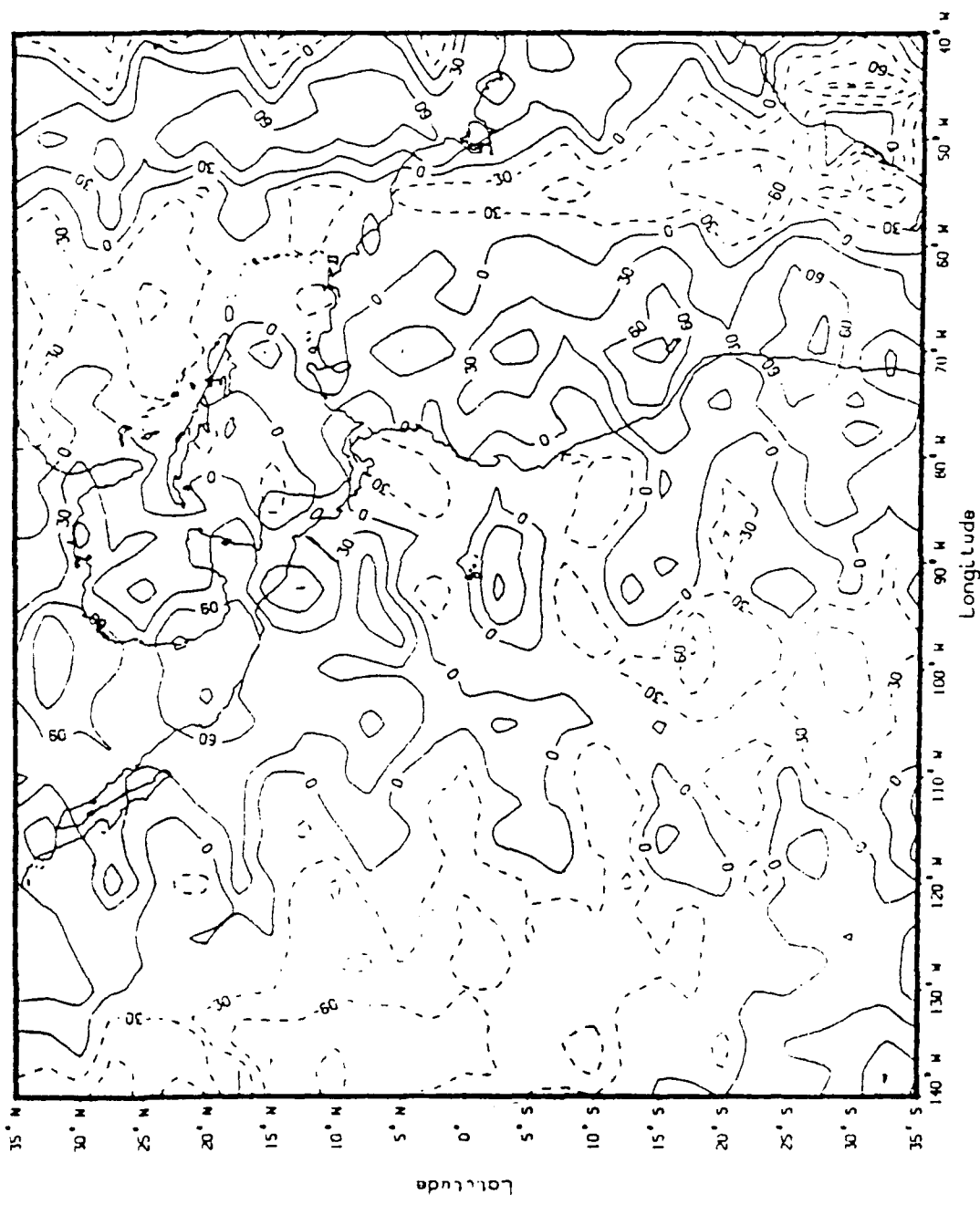


Figure 9. Composite diagram of Maximum OLR days in dry season (1 January - 9 May 1984). Contoured values represent deviations from seasonal averages in units of 10^{-1} Wm^{-2} .

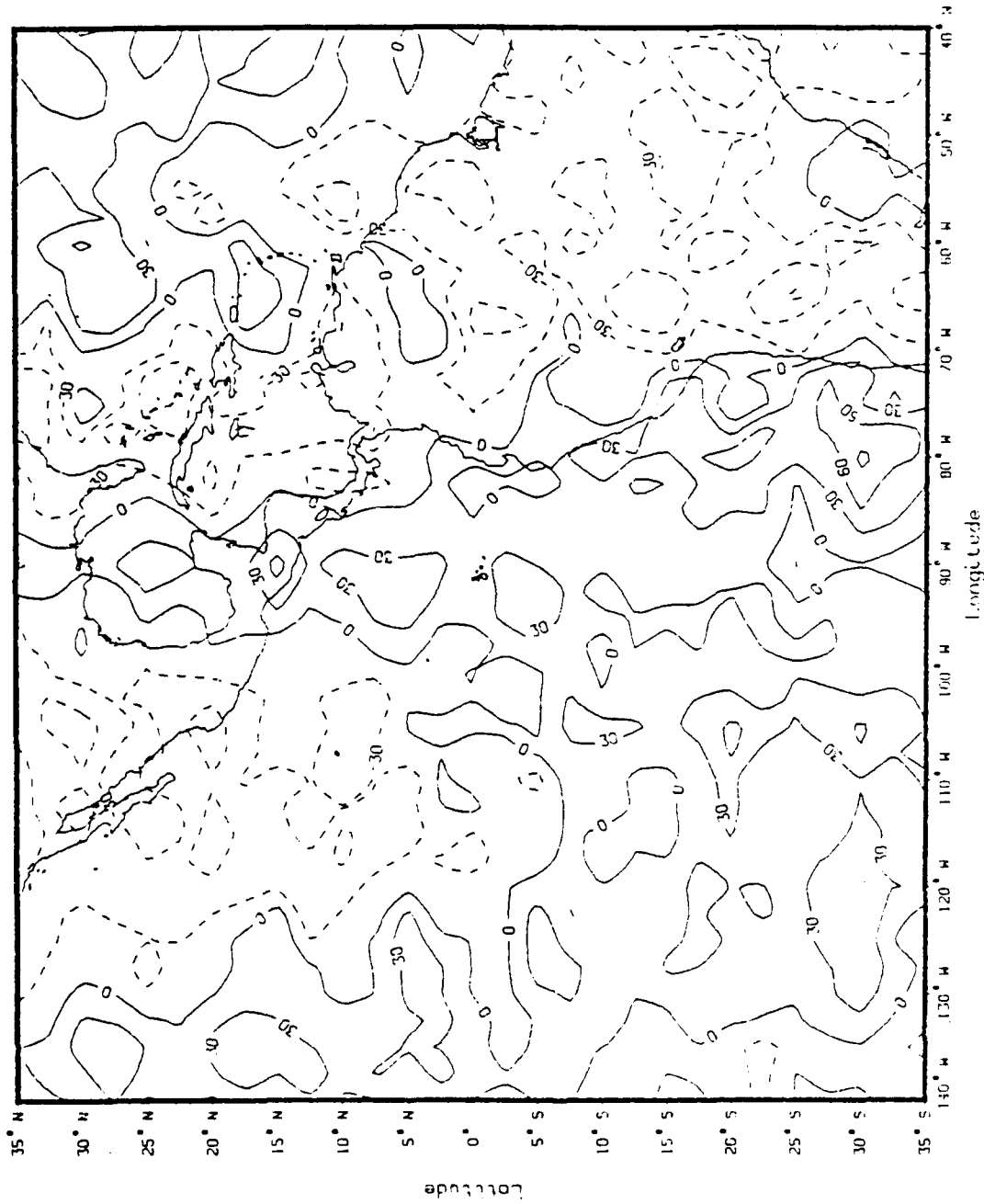


Figure 10. As in Fig. 9, except Maximum-to-Minimum OLR days.

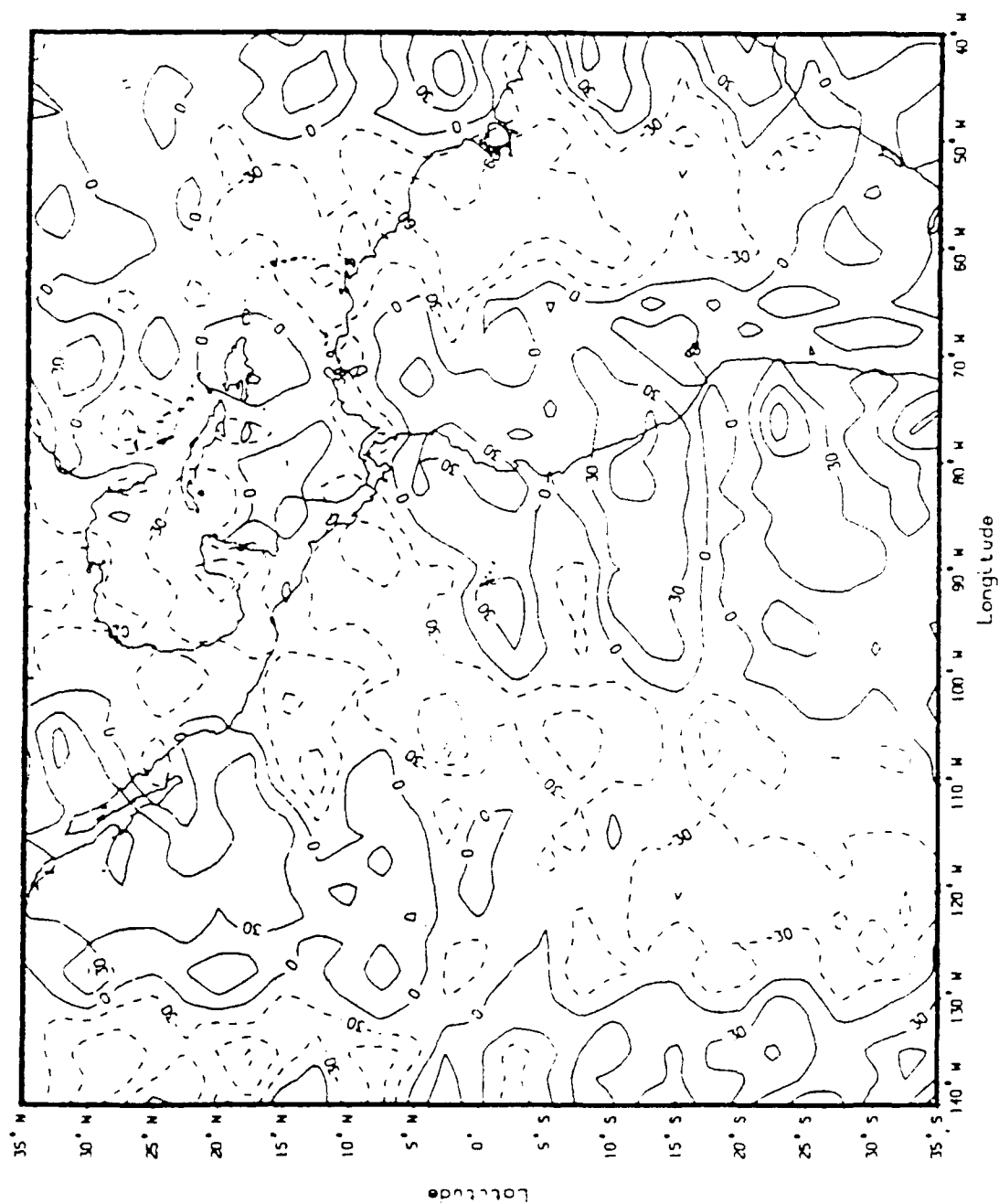


Figure 11. As in Fig. 9, except Minimum OLR days.

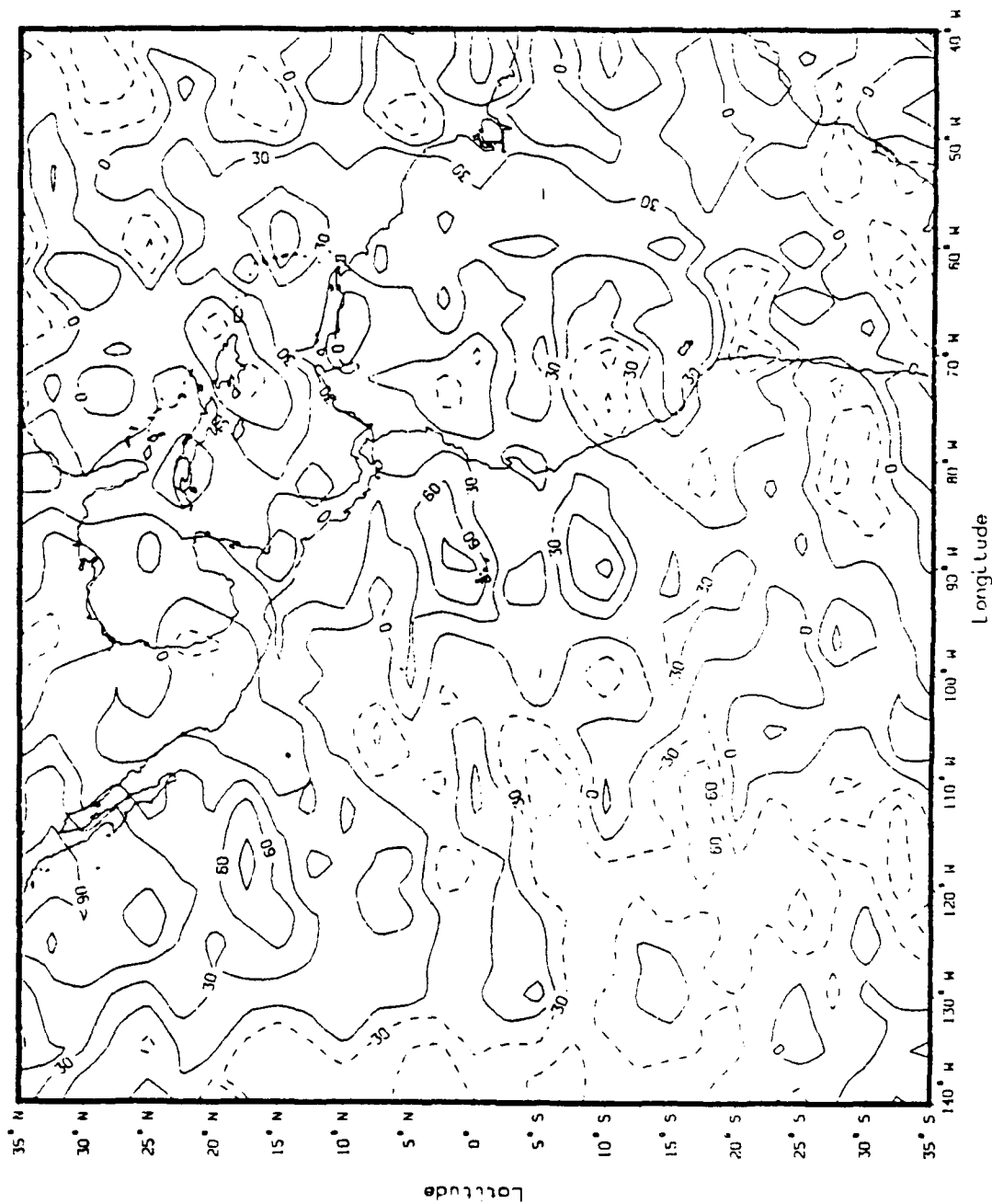


Figure 12. As in Fig. 9, except Minimum-to-Maximum OLR days.

Hemisphere. There is also a region of strong positive anomaly that has moved eastward in the northwestern part of the domain, and westward over South America. The result is an axis of positive anomalies along 85°W . Negative anomalies cover almost all of South America. Negative anomalies extend southward from the western United States to the equator.

Halfway through the 12 d oscillation (Fig. 11), the Minimum OLR composite indicates an overall strengthening of the positive anomaly areas but a major reduction in their areal extent. There is a suggestion of eastward movement and concentration of those areas, particularly over the north Pacific and the west coast of South America. The negative anomaly over the western United States has moved to the eastern United States and has extended across the equator all the way to 35°S at 120°W . The negative anomaly at 50°W observed in Figs. 9 and 10 has persisted to the Minimum OLR composite.

Finally, the Minimum-to-Maximum composite (Fig. 12) is remarkable for the extremely strong and widespread positive anomalies. These exist over and west of both North and South America. The motion of the axes of maximum OLR show consistent eastward movement over the continents.

The weak movement of the anomalies is consistent with that observed by Strager (1989). There are some notable differences in the strength and spatial extent of the anomalies. Figs. 9-12 have anomalies ranging from -9.0 to

+9.0 Wm^{-2} . The anomalies in Strager's composites (1989, Figs. 22-24) range -24 to +21 Wm^{-2} . The spatial distribution of the anomalies is not concentrated in a latitude band centered about Panama; rather, they appear to have a preferred meridional orientation throughout the domain. The striking difference between the the composites of these two studies is that the 12 d oscillation is readily apparent in the composites over Panama (Strager, 1989, Figs. 22-25). An examination of the filtered time series used by Strager (1989, Fig. 18) reveals that the days used in the phases of the oscillation are different than the days chosen for the present composites. The days chosen differ by 3-4 d. Once again, the spatial extent of the domain in the study must be recalled. Figs. 9-12 are indicative of 12 d oscillation over a domain larger than Strager's (1989) and not centered over Panama.

Individual days used to construct were compared with the composites and showed the same pronounced features observed in Figs. 9-12. The movement of the anomalies in Figs. 9-12 was verified through the construction and analysis of composite diagrams for the days before and the days after those used to obtain Figs. 9-12, giving daily continuity. Those diagrams (not shown here) show an eastward progression of the anomalies and the slow erosion in the meridional orientation of anomaly patterns as the features move eastward (particularly near 40°W).

Composite Diagrams for Wet Season

The complete cycle of the 12 d oscillation for the wet season is shown in the OLR anomaly composites in Figs. 13, 14, 15 and 16. As in dry season, there are strong anomalies present during the wet season phases. These anomalies are stronger than those present in the dry season. They have a similar meridional orientation. Arbitrarily beginning with the Maximum OLR composite (Fig. 13), there is a strong positive OLR anomaly over the American continents from 35°N to 10°S ; this positive anomaly extends south along 90°W . Negative anomalies are located over most of South America and the Pacific.

Three days later (the Maximum-to-Minimum composite, Fig. 14) the maximum anomaly located over the continents has weakened slightly but has extended both eastward and westward. The maximum anomaly at 90°W in the Southern Hemisphere has been replaced by maxima at 135°W and 75°W . The negative anomalies previously found over South America and the Pacific have weakened and decreased in areal extent.

In the Minimum OLR composite (Fig. 15) halfway through the 12 d oscillation, the Pacific and the meridional band near 60°W is dominated by positive anomalies. Negative anomalies are restricted to the Gulf of Mexico region and meridional bands at 70° and 110°W . However, the amplitudes of these anomalies dominate the composite.

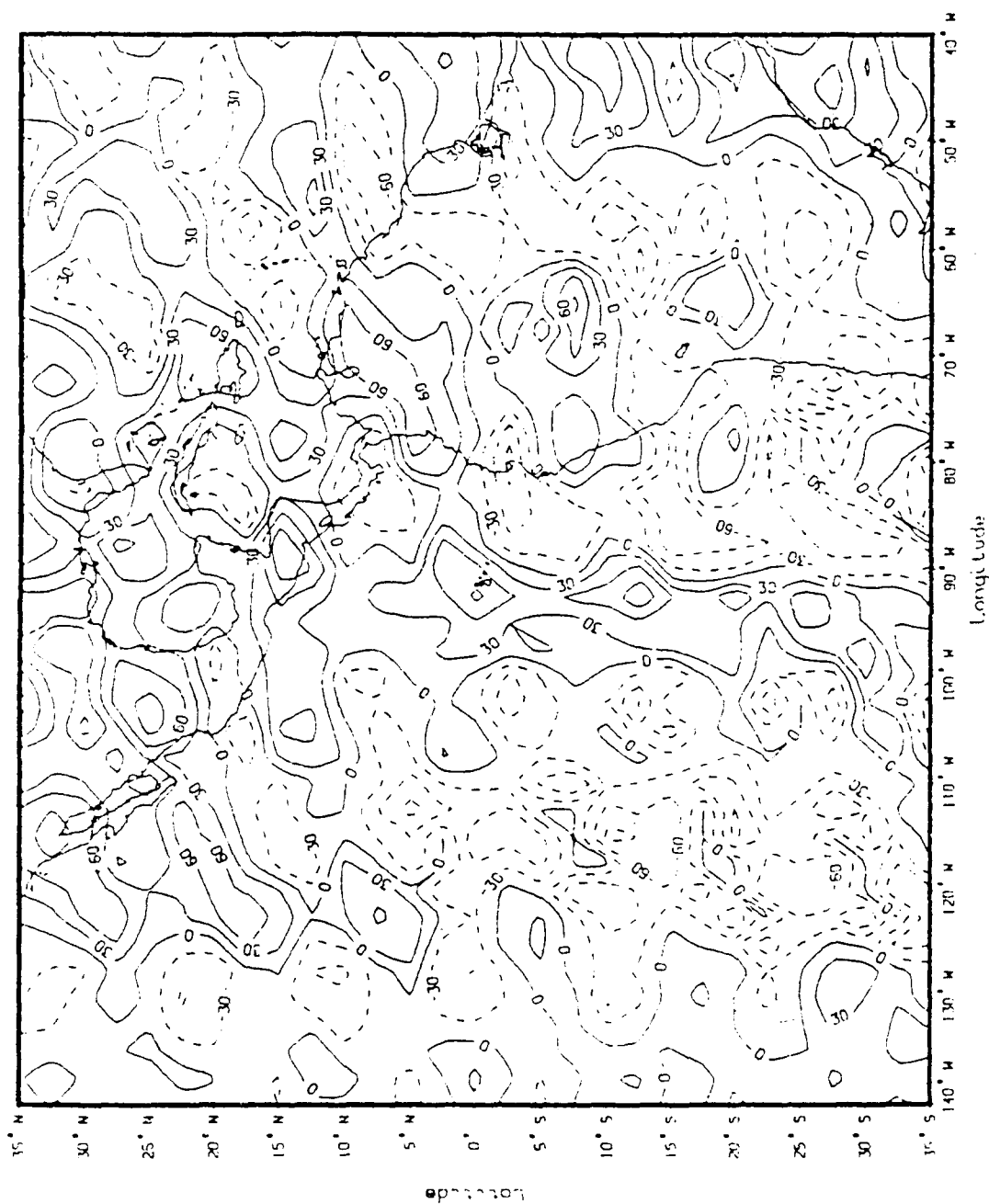


Figure 13. Composite diagram of Maximum OLR days in wet season (10 May - 4 December 1984). Contoured values represent deviations from seasonal averages in units of 10^{-1} Wm^{-2} .

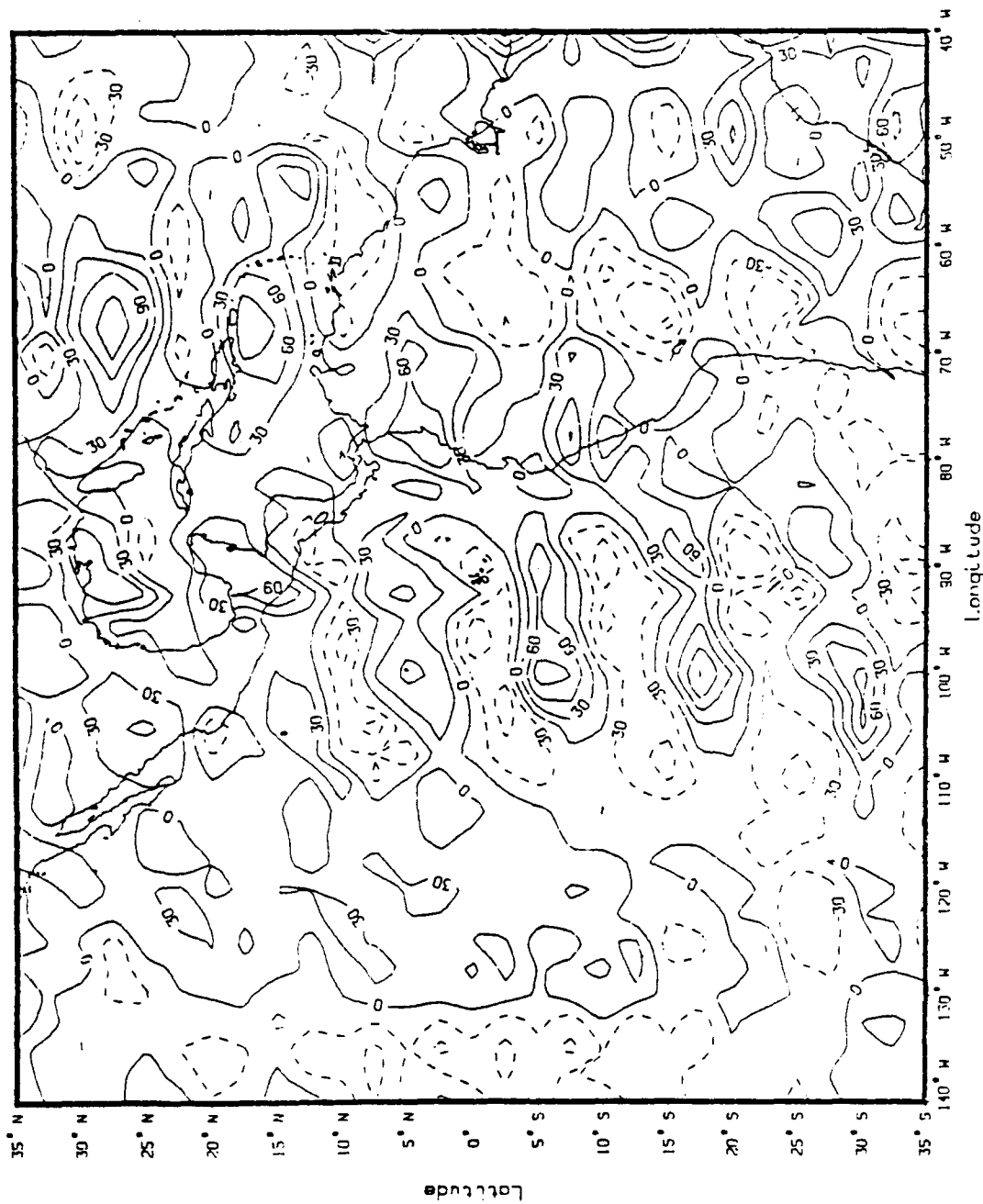


Figure 14. As in Fig. 13, except Maximum-to-Minimum OLR days.

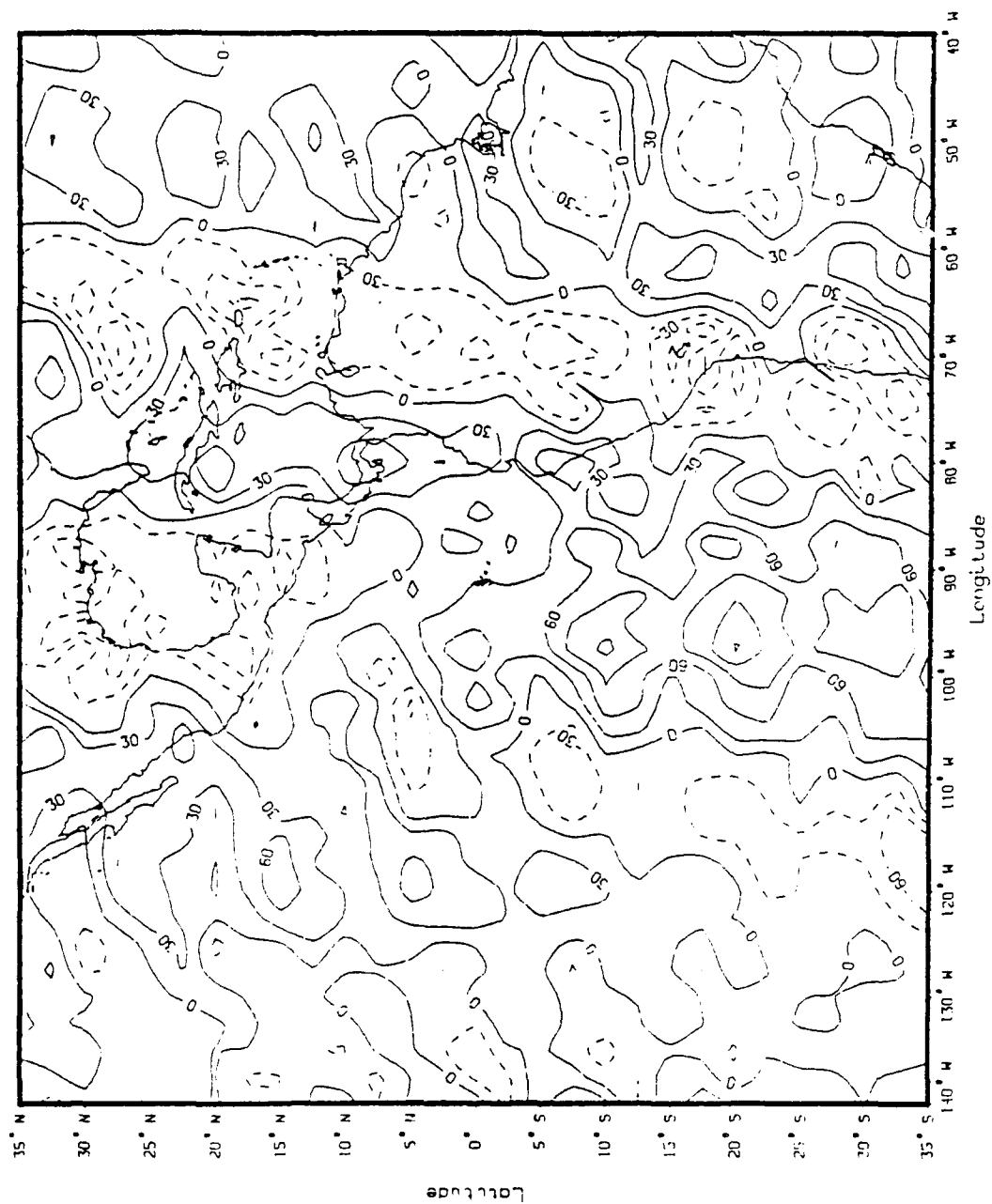


Figure 15. As in Fig. 13, except Minimum OLR days.

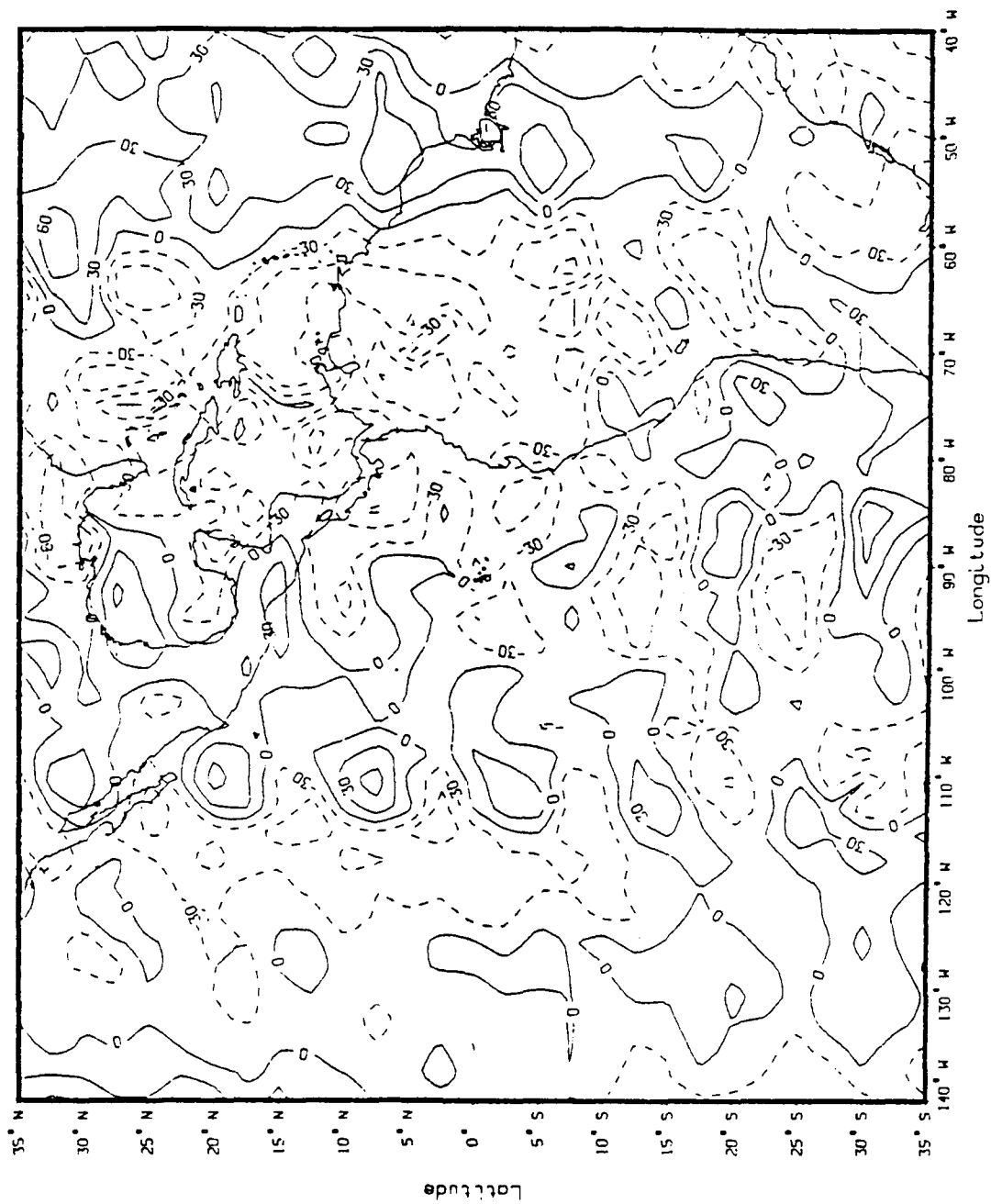


Figure 16. As in Fig. 13, except Minimum-to-Maximum OLR days.

In the last phase of the cycle (Fig. 16), there appears to be an increase in area and strength of the negative anomalies throughout the domain. The pattern is qualitatively similar to the pattern in Fig. 15, except the negative anomalies over the Pacific have moved slightly.

Again, the movement of the anomalies are similar to those observed by Strager (1989) while differing in strength and spatial extent. The range of the OLR anomalies in this study range from -9.0 to $+9.0 \text{ Wm}^{-2}$. The OLR anomalies in Strager's study (1989, Figs. 26-29) ranged from -21 to $+24 \text{ Wm}^{-2}$. The wet season OLR anomalies in this study were meridionally oriented as opposed to the latitude band-centered in the composites by Strager (1989). As in dry season, the filtered times series used by Strager (1989, Fig. 19) was examined to identify the days he used in constructing composites of the four phases of the oscillation. A similar difference of 3-4 d was observed.

As with dry season, the individual days used to construct the composites were compared with the composites. The meridional orientation of the OLR anomalies is evident in those composites as is the increase in their strength. The movement of the wet season OLR anomalies was deduced using composite diagrams constructed using the days before and the days after those used in Figs. 13-16. The time continuity diagrams (not shown here) show a westward movement in the anomalies and a continued meridional orientation.

The details and the actual pattern of anomaly movement are difficult to evaluate. First, many of the features appear to be nearly stationary, most particularly the meridionally oriented extrema. Secondly, unexplainable wavy (10° in the north-south direction) and (20° - 30° in the east-west direction) are a common feature in most of the composites, particularly in the wet season. They survive averaging over 9 and 10 composite days and they appear in most of the individual days of the composites. A particularly well defined example appears in Fig. 14 at 100°W . The explanation of these waves is unknown. Third, although large scale patterns in the dry and the wet seasons are similar, they do not evolve similarly. For example, in the dry season Maximum-to-Minimum composite (Fig. 10), the Pacific is dominated by positive anomalies. This feature occurs in the Minimum and Minimum-to-Maximum composites (Figs. 15 and 16) in the wet season. In the dry season, these warm (positive) anomalies replace a pattern of generally cold (negative) anomalies three days earlier; in the wet season, the warm anomalies seem to expand southward and propagate eastward over the cold anomalies six days earlier. Finally, even though filtered time series show systematic repeatable behavior, the pattern evolution lacks consistency in movement, amplification and expansion of anomalies. In spite of the detailed calculations of this 12 d periodicity, the

precise nature and explanation of the spatial pattern remains elusive.

In summary, the 12 d oscillation previously detected over Panama by Strager (1989) extends out into the east Pacific Ocean, the Caribbean and over South America. The wave seems to move eastward during the dry season. In the wet season, the direction of the wave probably changes to the west-northwest.

CHAPTER VI

ANALYSIS OF A 2800 KM THERMAL WAVE

Methods of Analysis

The TOVS data used in this study covered the period 1 January - 31 March 1984. The set consisted of randomly located observations of HIRS-2 Channel 3 (14.5 micrometers) brightness temperatures along the satellite track, spaced at approximately 300 km intervals. These observations were analyzed objectively onto a 2° latitude/longitude grid. The analysis procedure was a modified Barnes (1964) interpolation scheme. A maximum of 8 observations contributed to the analyzed value at each grid point; although most grid points used 8 values, in some data sparse regions, fewer than 8 observations were sufficiently close to the grid point to be used. In regions devoid of observations, spatial interpolation was used. An example of the interpolated gridded analysis is shown in Fig. 17. In Fig. 17, a tropopause is located at approximately 27°N and another is located near 25°S with warm readings poleward and colder observations within the tropical troposphere. The temperature range in the deep tropics is approximately 2 K and 6 K across the tropopause in the north-south direction. The synoptic scale seems well resolved. There is an apparent 3000 km wave in the zonal

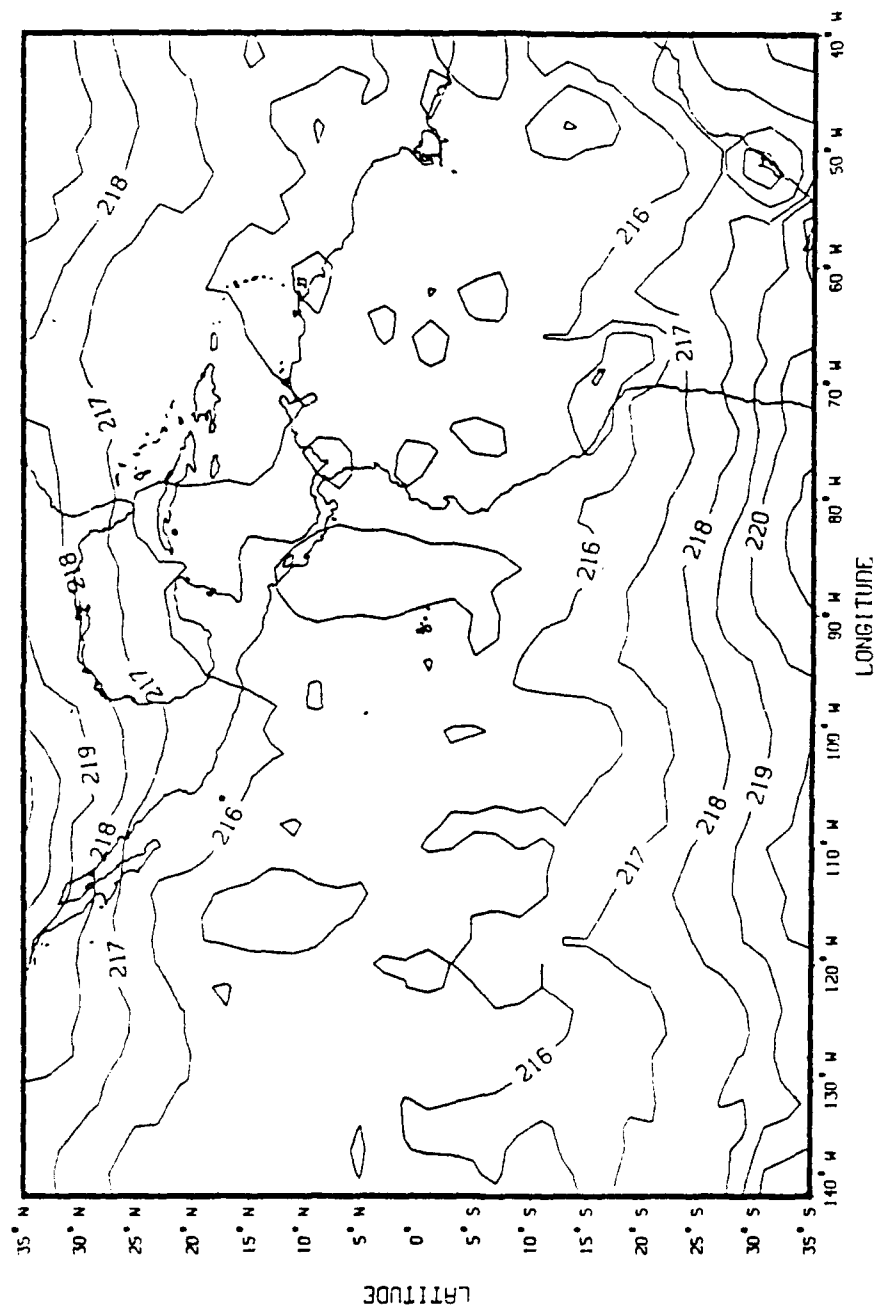


Figure 17. Analyzed HIRS-2 channel 3 brightness temperatures for 11 February 1984. Temperatures are in Kelvins(K) and contour interval is 1 K.

direction. Warm phases exist along the tropopause at 130° , 100° , 70° and 40° W in the Northern Hemisphere; cold phases appear at these longitudes in the Southern Hemisphere. The peak-to-peak amplitude seems to be about 1 K.

Non-linear Filtering

Schaefer (1988) identified an upper tropospheric thermal wave in a composite model of tropical plumes based on multichannel TOVS observations. This model consisted of 17 tropical plume events which occurred over the tropical northeast Pacific Ocean during the first three months of 1984. McGuirk et al. (1987) defined a tropical plume as a system characterized by a continuous band of upper and mid-level clouds at least 2000 km long, originating from a source equatorward of 15° N, and extending poleward of 15° N. The climatology of origin locations and origin times for tropical plumes in early 1984 is shown in Table 1. This climatology was developed independently by McGuirk and Ulsh (1990) based on definitions outlined by McGuirk et al. (1987). Schaefer's TOVS model was composed of two composited data sets. The first data set was the composite plume data set consisting of 21 satellite radiance channels (several channels were removed before the analysis, as described by Schaefer, 1988). The events were composited for 13 consecutive 12-h time periods spanning the pre-plume state, plume evolution and plume

Table 1. List of tropical plumes and their origins used in the tropical plume composite. After Schaefer (1988).

Event No.	<u>Definition</u>		<u>Origin</u>	
	Date (1984)	Time GMT	Lat (°N)	Long (°W)
1	1 Jan	2316	8	127
2	3 Jan	0515	6	150
3	7 Jan	2316	5	156
4	18 Jan	0515	13	136
5	21 Jan	2316	12	128
6	22 Jan	2316	7	148
7	26 Jan	1115	5	157
8	2 Feb	0515	6	140
9	9 Feb	0515	7	157
10	17 Feb	0516	10	120
11	17 Feb	2316	0	158
12	22 Feb	1115	7	153
13	3 Mar	1115	6	128
14	8 Mar	0515	6	125
15	11 Mar	1115	12	120
16	16 Mar	1615	4	140
17	25 Mar	1615	6	130

dissipation. A zero reference point (0° latitude/longitude) was set at the southwest edge of the tropical plume cloud band where it intersected the ITCZ. The second composite set contained time periods (Table 2) in which no tropical plumes were observed to exist. Since there were no longitudinal reference points for these cases, the zero point longitudes were all set to 145°W . The zero point latitudes were set between 0° - 8°N at the approximate latitude of each day's mean position of the ITCZ (These events are a subset of the quiescent composite set as defined and used by McGuirk and Ulsh, 1990.).

The set of brightness temperatures forming the composites were synthesized using empirical orthogonal function (EOF) analysis. Two procedures added to the EOF analyses contributed to the identification of a small synoptic-scale wave in upper tropospheric temperatures: 1) The mean climatological state was removed prior to analysis of channel radiance data. This reduction allowed smaller scale variance structures to become relatively more important; 2) The individual days of the composites were aligned with respect to a common feature--the origin point of the a tropical plume. The upper tropospheric wave also appeared to align itself with respect to the plume initiation. The EOF analysis implied that the vertical structure of the wave appeared as the third vertical mode: There are three extrema, at 300, 700 and 900 mb, in the vertical temperature

Table 2. Dates and locations selected for quiescent composite. No tropical plumes were evident. After Schaefer (1988).

No.	Date (1984)	Time GMT	Origin	
			Lat (°N)	Long (°W)
1	19 Jan	1616	8	145
2	31 Jan	2316	5	145
3	4 Feb	1616	7	145
4	6 Feb	2316	8	145
5	15 Feb	1616	4	145
6	20 Feb	1615	5	145
7	1 Mar	2315	1	145
8	4 Mar	1615	7	145
9	6 Mar	1615	3	145
10	10 Mar	2315	3	145
11	12 Mar	1615	3	145
12	28 Mar	1615	2	145
13	29 Mar	2315	5	145

distribution. The diurnal signal was a significant feature in nearly all channels. Schaefer (1988) used non-linear regression of appropriately filtered TOVS brightness temperatures to document the quantitative structure of the upper tropospheric wave. The non-linear regression allowed him to take full advantage of the known properties of the wave: Its existence; its mean wavelength of 2800 km; its appearance in only certain TOVS channels (about 60% of them); and, its differing behavior at different latitudes. He applied non-linear regression to all the TOVS channels within several latitude bands and throughout the tropical plume composite evolution. The resulting wave characteristics are provided here: 1) For the composite tropical plume the wave maintains a consistent configuration and movement throughout the important time periods of the plume's development. 2) The tropospheric wave either tilts baroclinically to the west with height or is equivalent barotropic (no vertical tilt); it is positioned such that the maximum low level instability lies just to the east of the origin point at origin time.

To verify the existence of the 2800 km thermal wave in the channel 3 brightness temperatures for the same three month period used by Schaefer (1988), the non-linear recursive band-pass filter described and used in Chapter V on the OLR time series was applied to the gridded TOVS data set. The filter was used spatially to identify zonal waves along fixed latitude lines. The central wavelength of the filter

in this study was 28° longitude (full response) and the half amplitude points were 20° and 36° longitude wavelengths. The central wavelength and the half amplitude points were chosen to fit a 2800 km wave on the TOVS gridded data described by Schaefer (1988). The filter was applied to gridded Channel 3 data along seven latitude bands for each day of the study: 1° , 5° , 9° , 15° , 19° , 25° , and 33° N. The zonally filtered data were used to construct Hovmoller diagrams (longitude vs. time) for each of these latitudes and are shown in Figs. 18-24. In these diagrams only the isopleths for negative temperature anomalies are shown, in order to maintain clarity. There are two time periods in each figure where there are missing TOVS data - days 18-21 and 78-84. Because of the interpolation for analysis purposes, the isopleths during these periods appear as vertical lines, constant in time; they have no physical meaning.

In all the figures, Figs. 18-24, there appears to be a wave of approximately 2800 km, moving eastward at approximately $5-8 \text{ ms}^{-1}$. However, examination of Figs. 18-24, particularly between 9° and 25° N, show results too good to be true. There is a marked regularity and periodicity to this wave. The only ways such a phenomenon could appear in atmospheric data are: i) It is a construct of the analysis procedure; ii) it is a result of regularity in the observation procedure; or, iii) it is a feature forced by a strong, highly-periodic atmospheric forcings; such as a

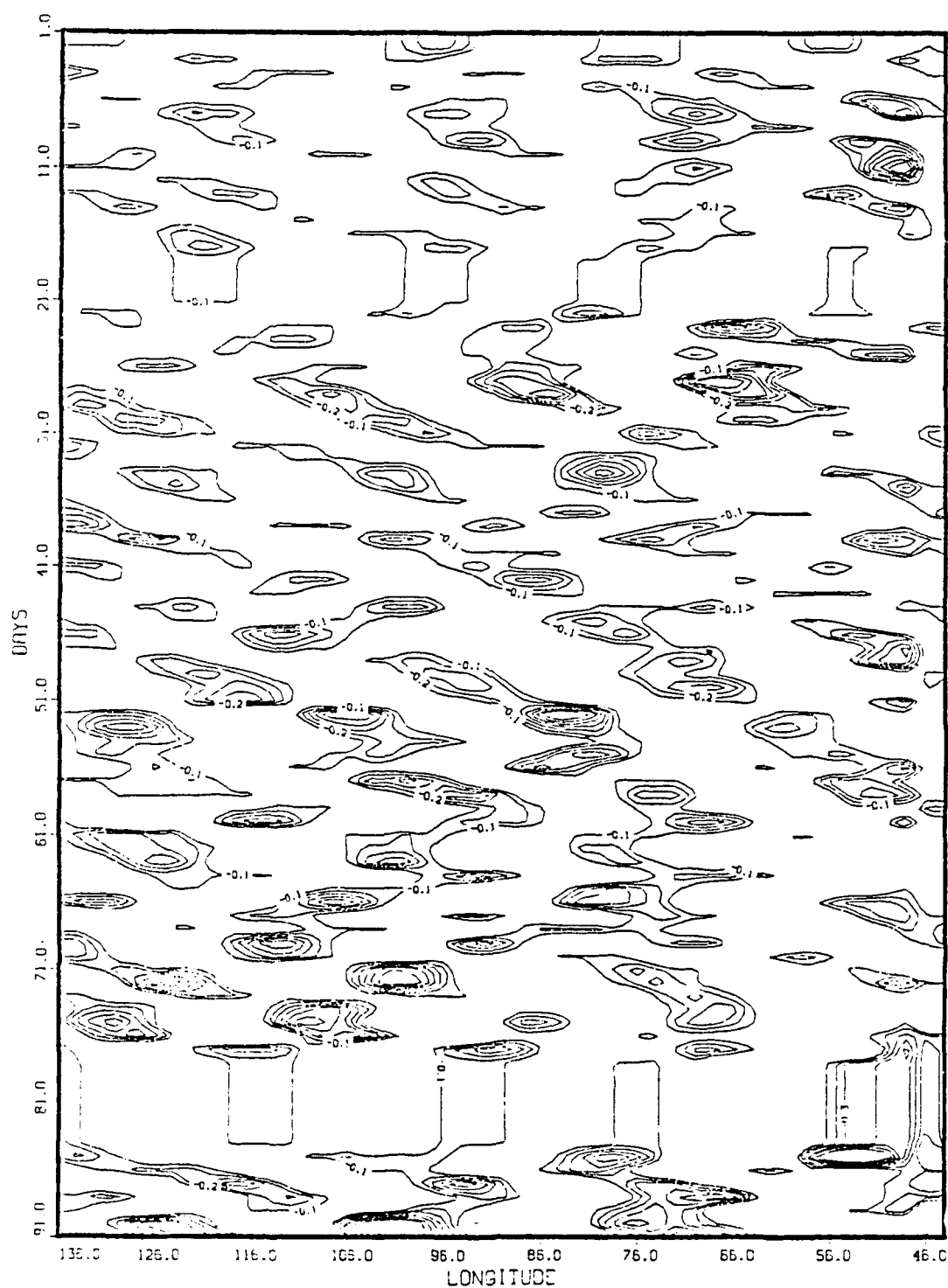


Figure 18. 28° longitude filtered channel 3 brightness temperatures for 1 January - 31 March 1984 centered at 1°N over 136°-44° W in units of Kelvins.

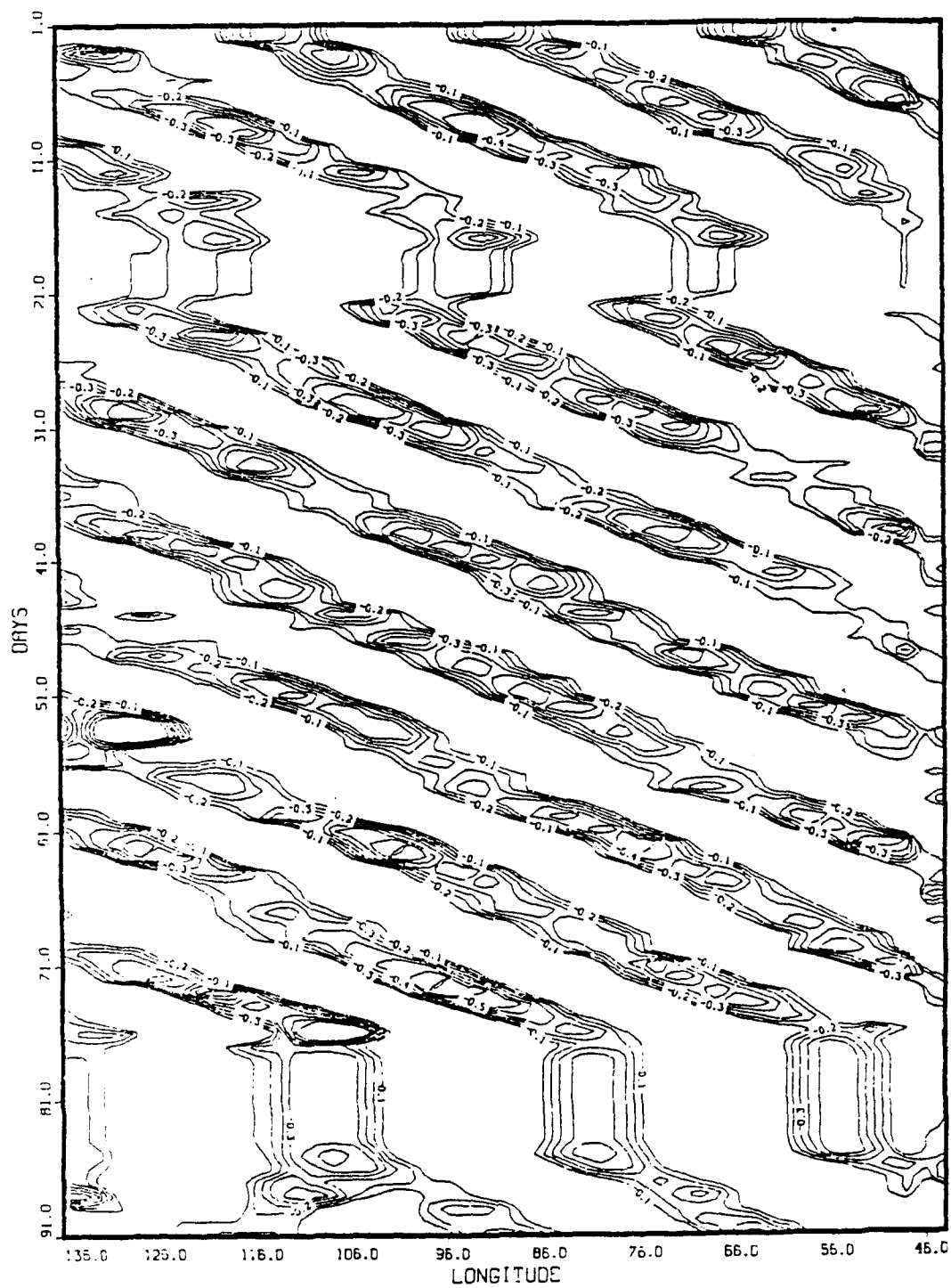


Figure 21. As in Fig. 18, except 15°N.

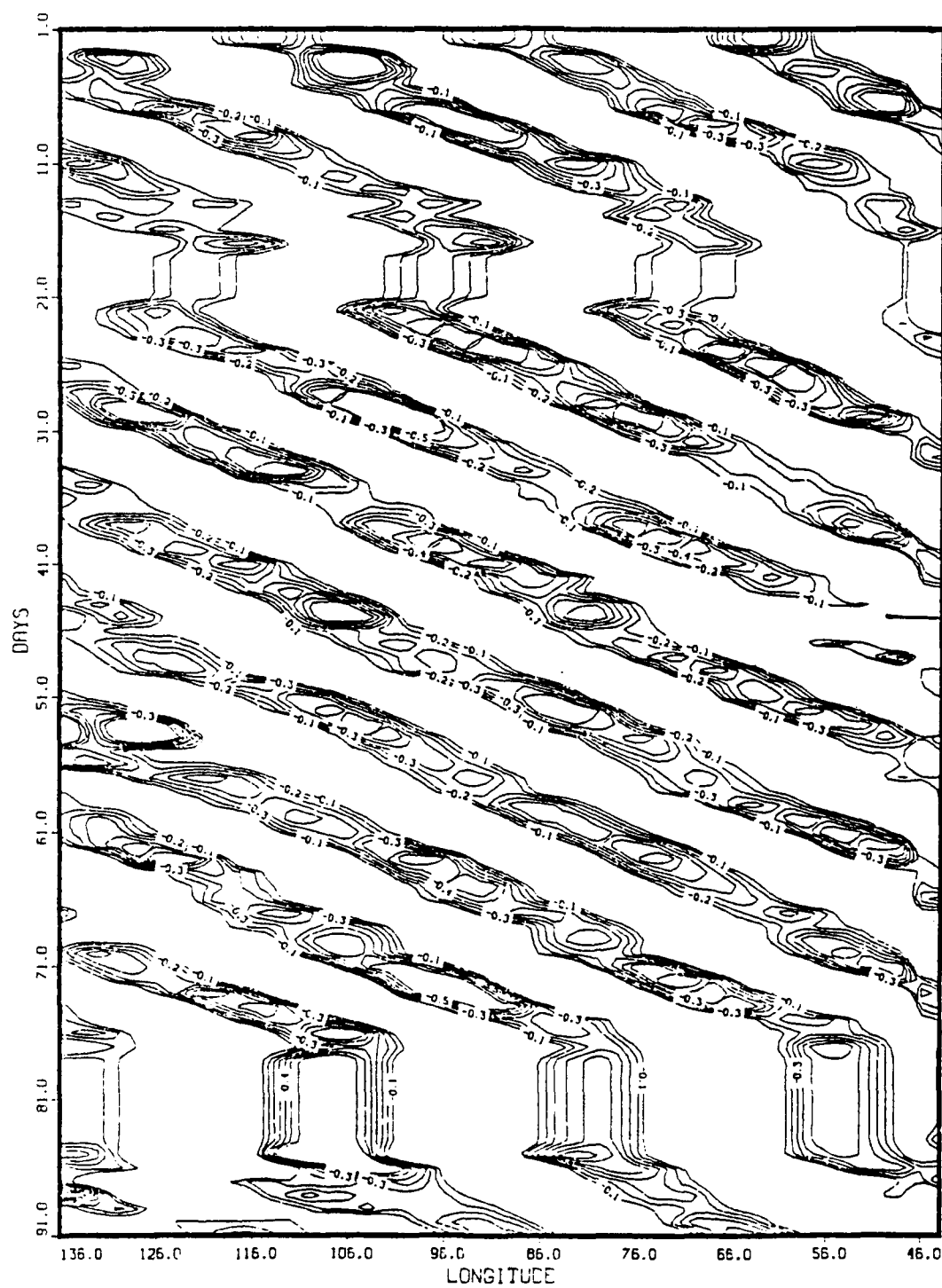


Figure 22. As in Fig. 18, except 19°N.

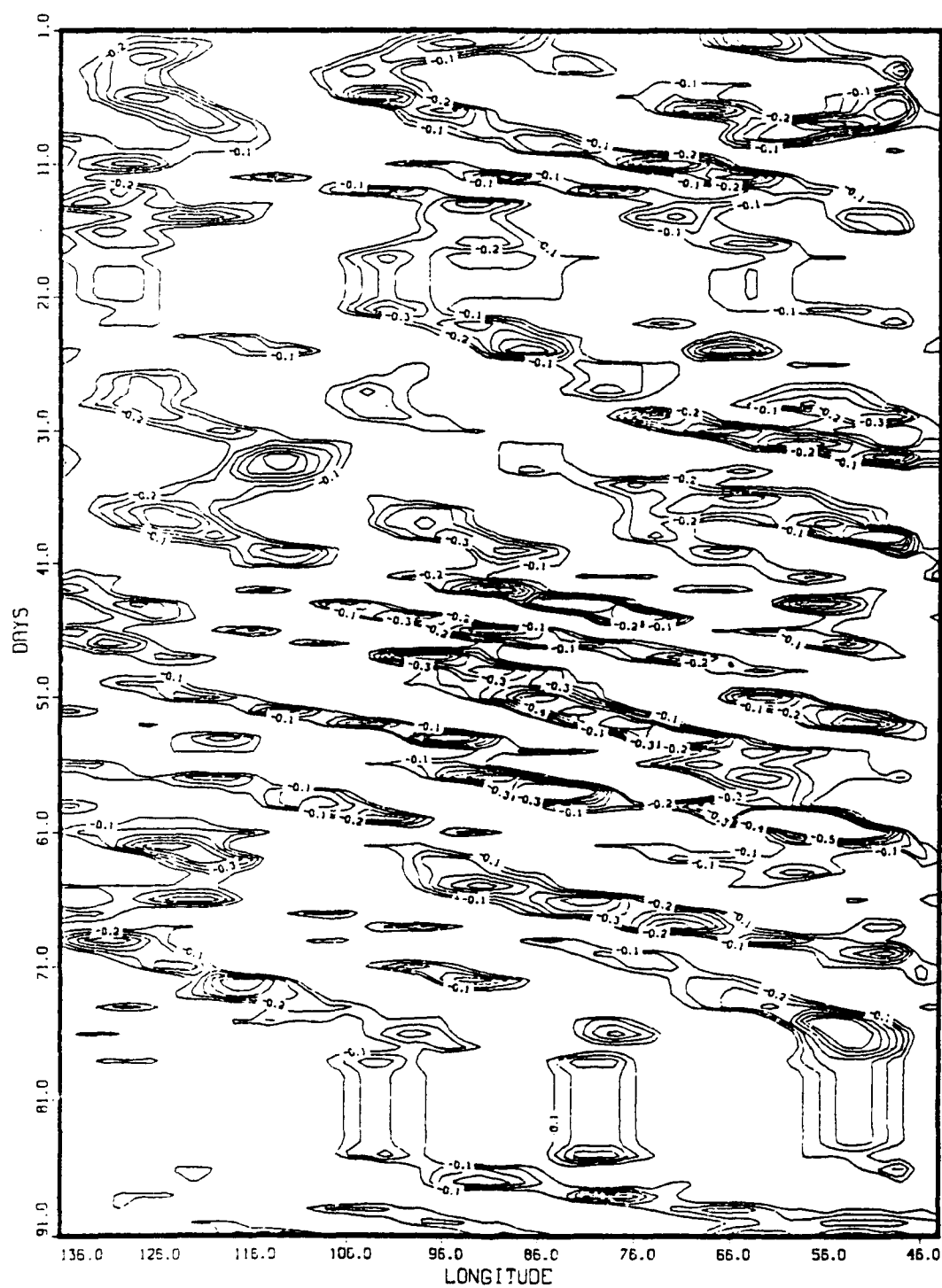


Figure 24. As in Fig. 18, except 33°N.

diurnal or annual cycle. Regarding (iii), no geophysical phenomenon is known to exist with forcing properties which would lead to such a propagating wave result. Regarding (i), the filter used has been well documented and possesses no biases that would operate on individual days of the analysis. The data of consecutive days are independent, at least insofar as the filter analysis procedures are concerned. These conclusions suggest an observational bias, related to systematic behavior of the satellite observation suite.

The path width of the polar orbiting NOAA-7 and NOAA-8 satellites is about 25.3° longitude. Viewing the atmosphere from satellite is somewhat different at the sub-satellite point (or nadir) and at the edge (or limb) of the satellite swathe. The optical path at the limb is somewhat larger than at nadir. This difference causes the peak in the weighting function for each satellite channel to be shifted upward in the atmosphere. For tropospheric channels, limb observations will read cooler than nadir observations because of a lapse rate effect. This cooling is referred to as "limb darkening". Because of the reversal of the lapse rate in the stratosphere, stratospheric satellite channels experience "limb brightening". Although operational procedures correct for a climatological limb darkening effect, small local limb darkening effects remain in the observations.

Limb darkening is a particularly insidious problem in that there is always the possibility that any real at-

mospheric signal with a wavelength similar to the separation distance between adjacent satellite passes (25.3° longitude, or about 2800 km at the equator) inevitably will be aliased by the satellite sampling characteristics. Therefore any signal of this wavelength must be investigated carefully to determine if the pattern is a result of meteorological factors, or a result of the operational characteristics of the satellite. Schaefer (1988) was aware of limb darkening problems. He applied a regression technique used by Anderson (1986) in TIROS-N observations to evaluate SCan Angle Bias (SCAB) error on the 1984 NOAA-7 and NOAA-8 observations. The analysis resulted in a statistically insignificant regression with small amplitude coefficients. He concluded that no significant SCAB problem existed in the NOAA-7 and NOAA-8 data set.

In his study, Schaefer (1988) excluded limb brightening/darkening as a significant contaminant to the analysis. The following evidence was presented:

1. Each daily analysis was constructed from satellite data observed over a 12-h period. Generally, observations contributing to the analyzed brightness temperatures at a gridpoint could come from as many as five different satellite passes -- adjacent passes, ascending and descending passes, and passes from two different satellites. Such a collection of observations would inevitably smear out any limb darkening effect. (Comment: While this is true for more polar

latitudes where the overlap of satellite passes is much greater, orbital mechanics of the satellites keeps the orientation of satellite passes constant with respect to each other. Therefore some residual systematic limb darkening effect is possible.)

2. The wave amplitudes of the 2800 km wave associated with individual plumes were considerably weaker for nighttime satellite passes. While there may be slight differences in the amplitude of the limb brightening/darkening between ascending and descending passes, the difference would be minimal.

3. The wavelength of the 2800 km wave varied considerably as the tropical plume matured and dissipated. (Comment: This effect must be considered a meteorological signal.)

4. The speed of the wave could not be accounted for by movement of the equatorial crossing longitudes of the satellites (which progress eastward at 1.28 ms^{-1}). (Comment: While this is true, it is still erroneous logic. Since the satellite orbital period is not an integral multiple of 24 h, the satellite track appears to progress eastward at about 5 ms^{-1} , moving a full swathe width every few days. The "apparent" phase speed is suspiciously close to $4\text{--}8 \text{ ms}^{-1}$.)

5. The distinct pattern associated with ascending/descending passes that described limb darkening found by

Anderson (1986) was not present and was not removable by the SCAB correction.

6. The vertical structure of the thermal wave could not be explained by limb darkening. (Comment: This argument is only partially correct. There was a shift from warm to cold in the mid and lower troposphere that could not be accounted for by limb darkening. However, the primary structure in the upper atmosphere could easily be explained by the shift from limb darkening to limb brightening in the stratosphere.)

7. There was no preferred location, in time or longitude, of the equatorial crossing longitude of the satellite with respect to the tropical plume origin. If the thermal wave was a statistical resultant of limb brightening/darkening there would not be a systematic association between the equatorial sub-satellite point and the plume/thermal wave complex. No such systematic behavior existed. The thermal wave is always positioned with respect to the plume origin, a distinctly meteorological effect.

While some of his reasoning is incorrect, the fact remains that regardless of the presence of limb brightening/darkening, a 2800 km thermal wave seems to exist. At issue is whether the 2800 km wave is a satellite observational bias or a meteorological feature. The properties of Figs. 18-26 suggest that limb darkening must be a strong contaminant. The observations 3 and 7 above, linking the thermal wave to plume features, suggest that a real meteor-

ological phenomenon exists. Because of limb darkening, the TOVS data set is not conducive to identifying such a wave or describing its characteristics.

Non-linear Regression

An attempt was made to remove the limb darkening effect through a simple statistical correction, much the same way as Schaefer (1988) attempted to remove SCAB. Non-linear regression fits observed data to an arbitrary function specified by the analyst. The fitting merely estimates parameters within the chosen function. The difference between linear and non-linear regression is that, in the latter, the parameters enter the function in a more complicated, non-linear fashion.

A computer routine that invokes a user-supplied function to perform non-linear regression is provided in the IMSL User's Manual (1987). The function selected in this case is:

$$F = A \cos \left[2 \pi \left(\frac{x - ct - d}{x_0} \right) \right]$$

where: F is the function

A is the amplitude

c is the propagation speed

d is an arbitrary phase shift

x_0 is the wavelength

x is the observation point

and t is the observation time.

and t is the observation time.

The variables determined by the regression will determine such features as the location, speed, amplitude and wavelength of the wave, independent of any researcher bias. In this non-linear regression, an iterative procedure is invoked in which first guess values are inserted for each of the parameters. The final estimated values of the parameters can be sensitive to the first guess. For example, x_0 was initialized at 2800 km. If a wavelength was considerably different from the selected value, the non-linear regression presumably would have selected out a different Fourier component and fitted the parameters to that component. Parameters for F were estimated from the data for the Hovmoller plots in Figs. 18-24. Data at all latitudes were pooled. The resulting function specified an approximate limb correction, for mean January through March conditions. Only significant synoptic variations, meridional variations due to latitudinally varying limb effects or synoptic structure, or long term (seasonal) trends would remain.

The amplitude determined by the regression and its spatial-temporal dependence was deducted from the band-pass filtered TOVS data in an attempt to remove the apparent observational bias. Hovmoller diagrams were again constructed for the modified latitude-centered series. The results are shown in Figs. 25-31. Figs. 25, 26 and 27 seem to present some random possible synoptic events. However,

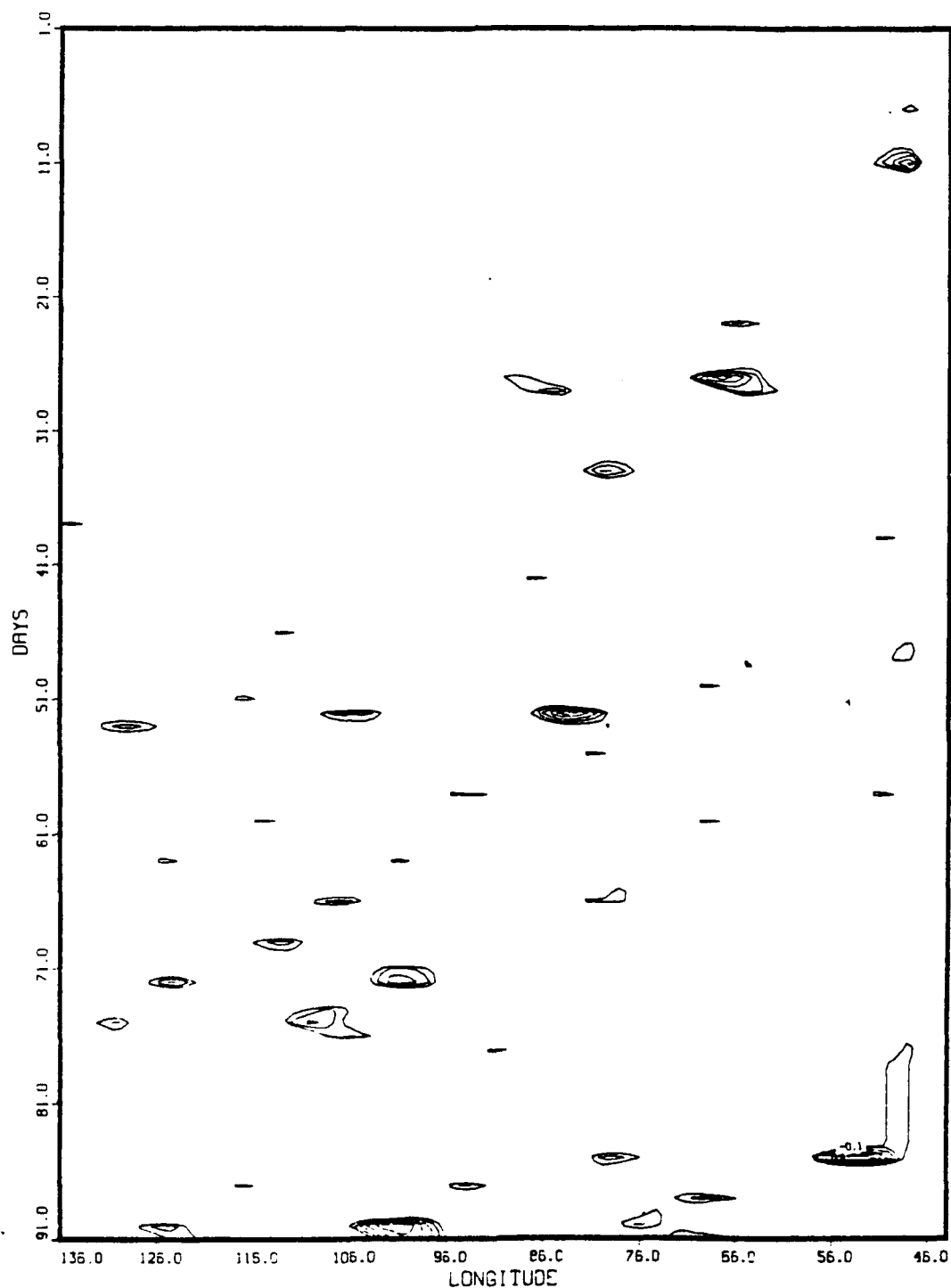


Figure 25. Results of non-linear regression on 28° longitude filtered channel 3 brightness temperatures for 1 January - 31 March 1984 centered at 1°N over 136°-44°W in units of Kelvins.

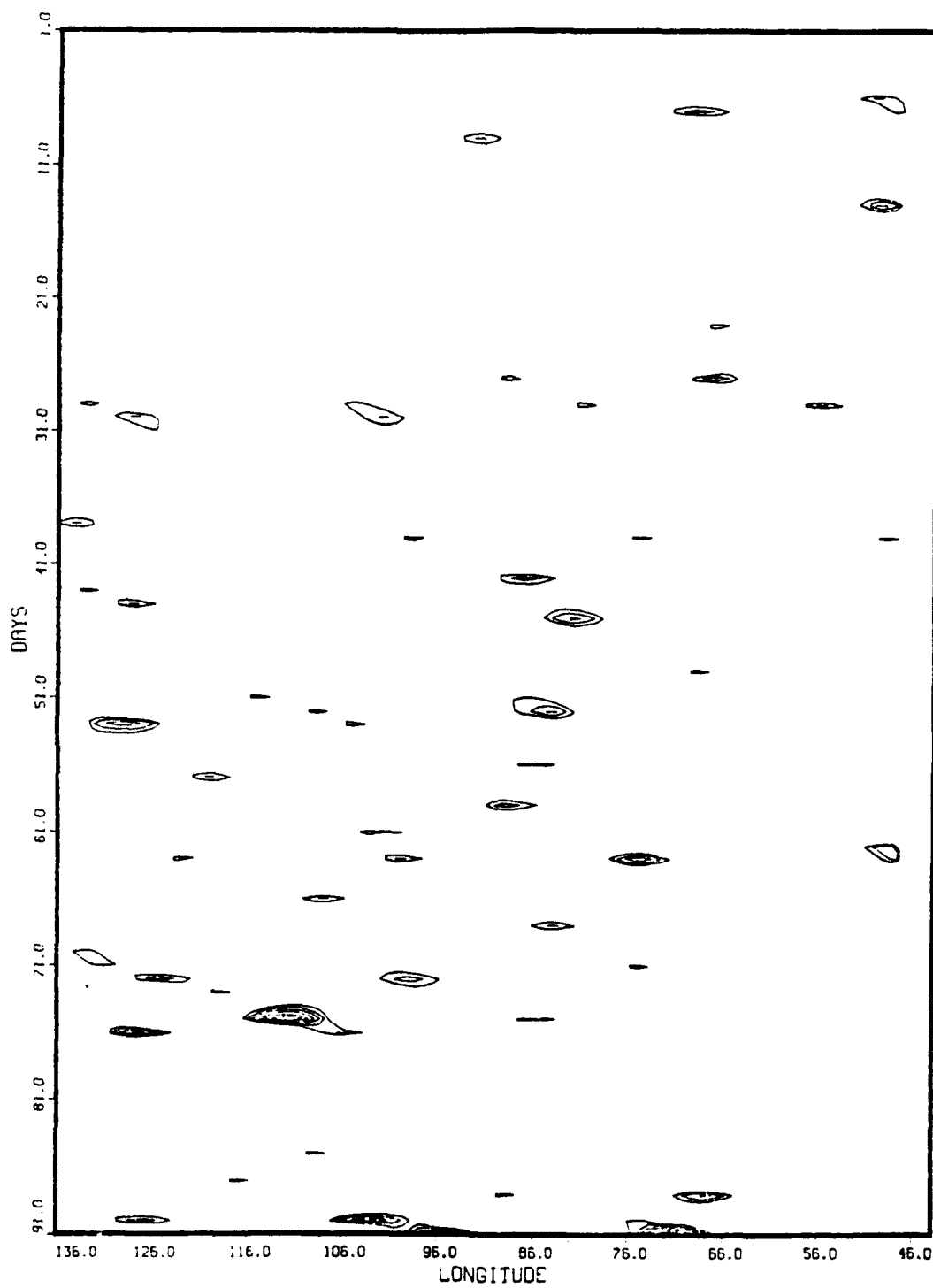


Figure 26. As in Fig. 25, except 5°N.

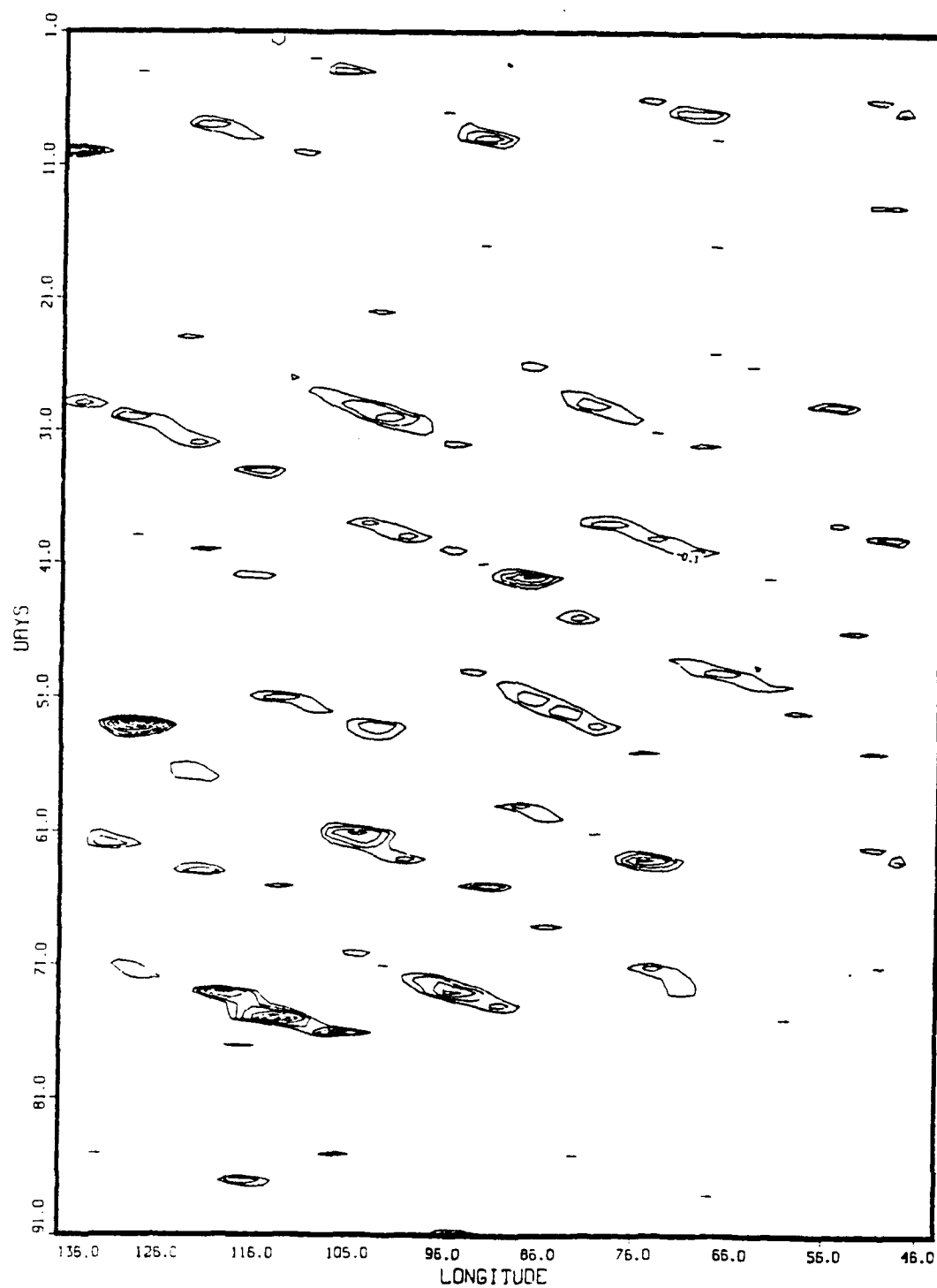


Figure 27. As in Fig. 25, except 9°N.

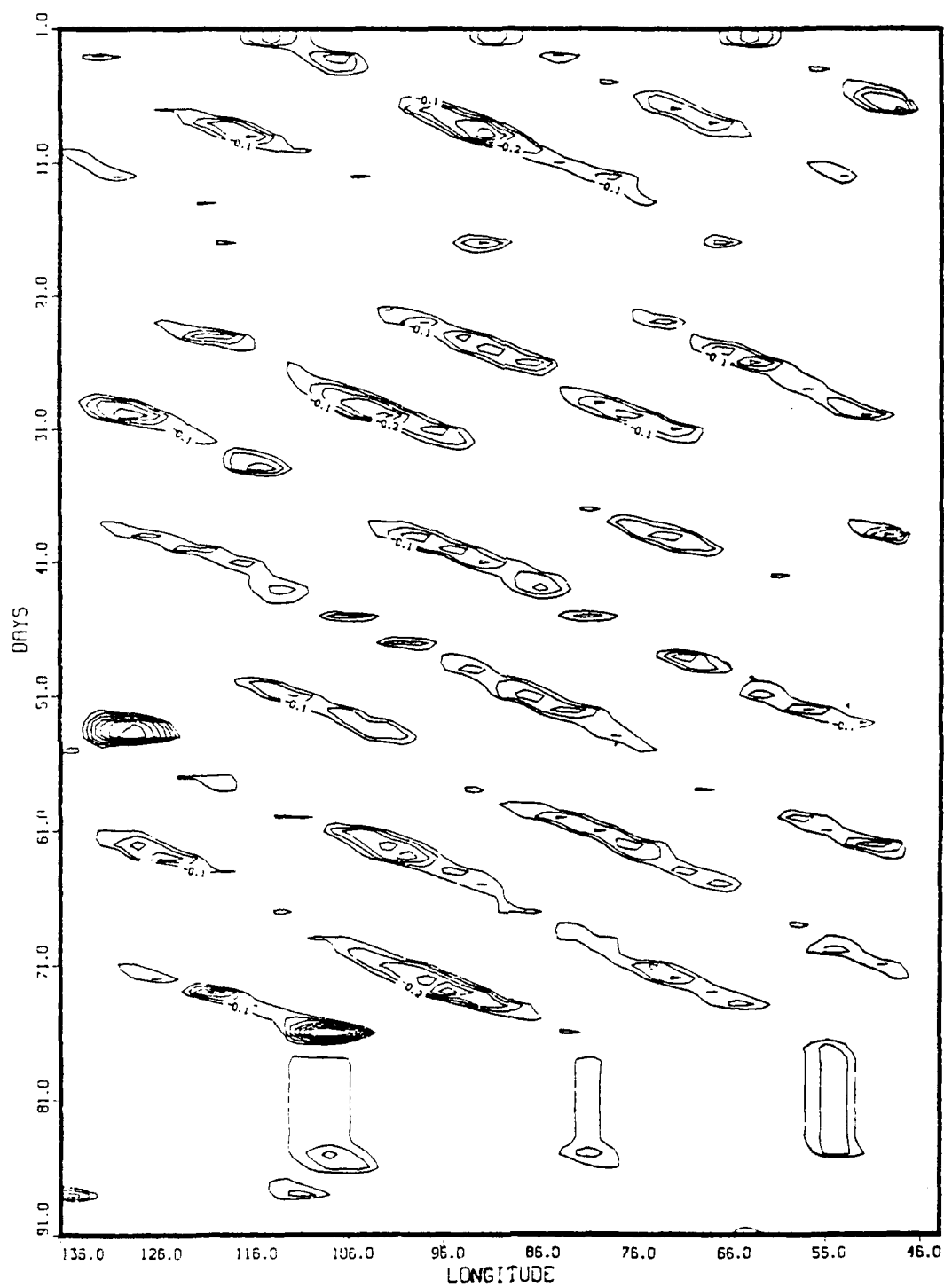


Figure 28. As in Fig. 25, except 15°N.

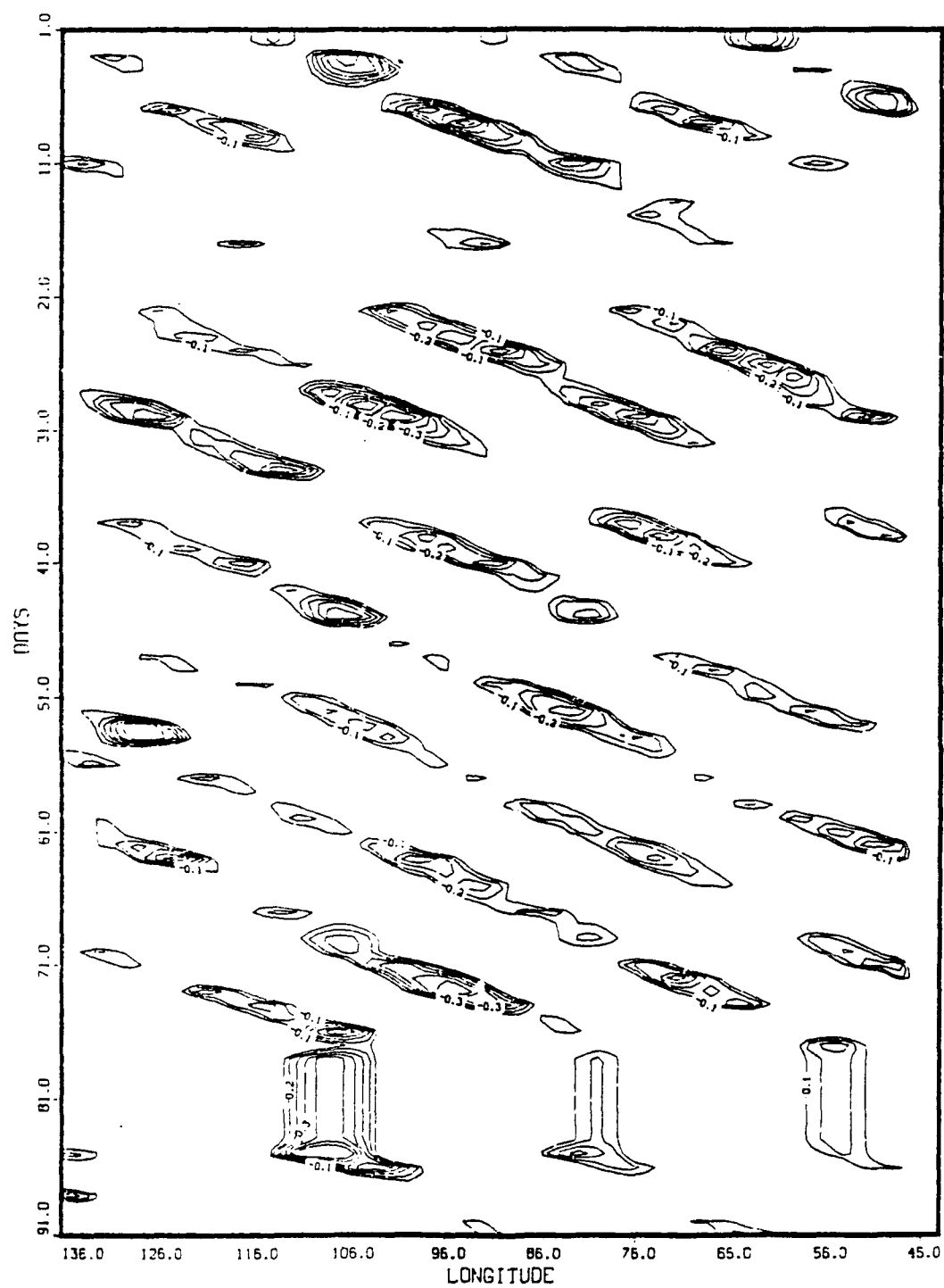


Figure 29. As in Fig. 25, except 19°N.

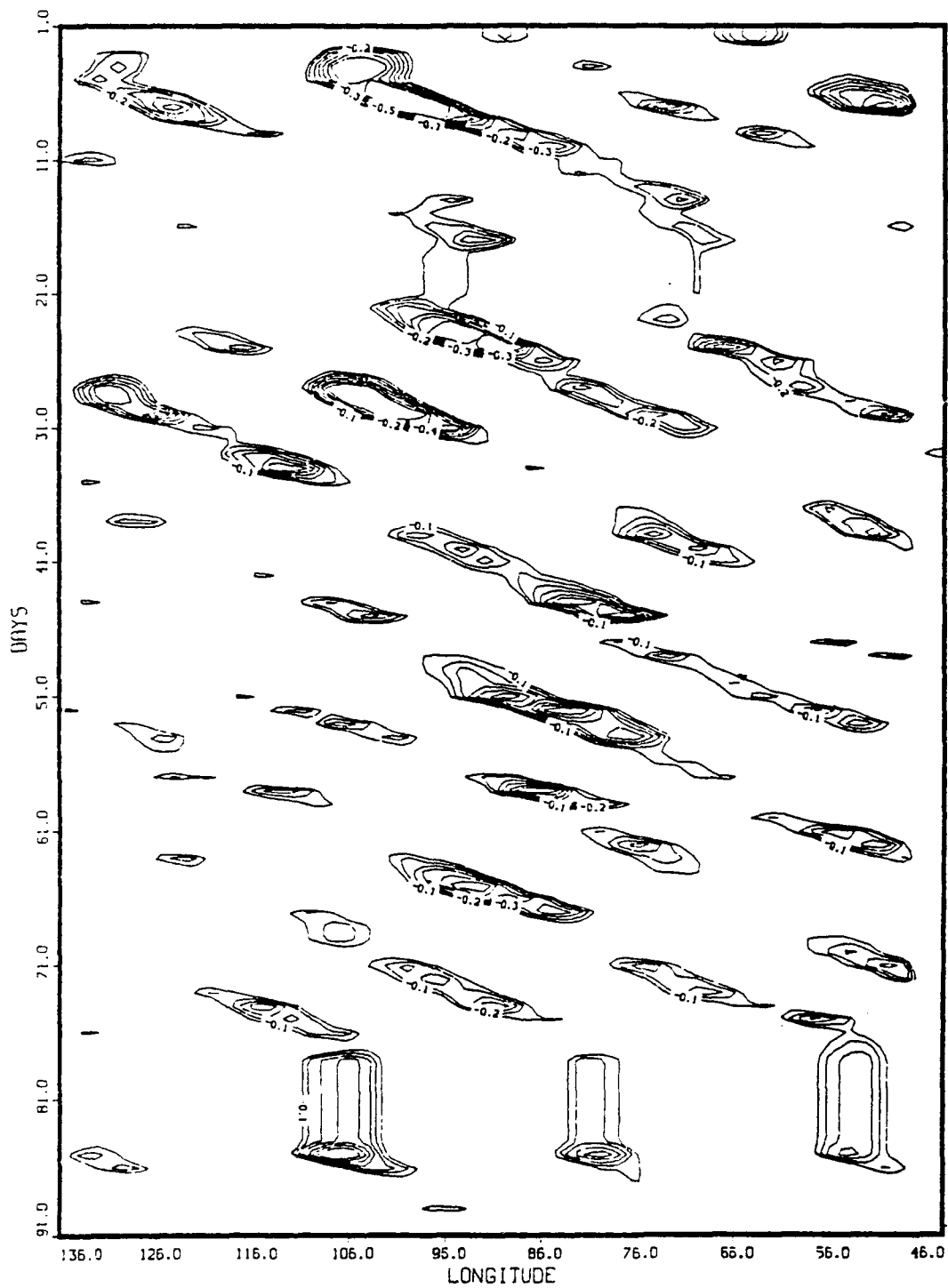


Figure 30. As in Fig. 25, except 25°N.

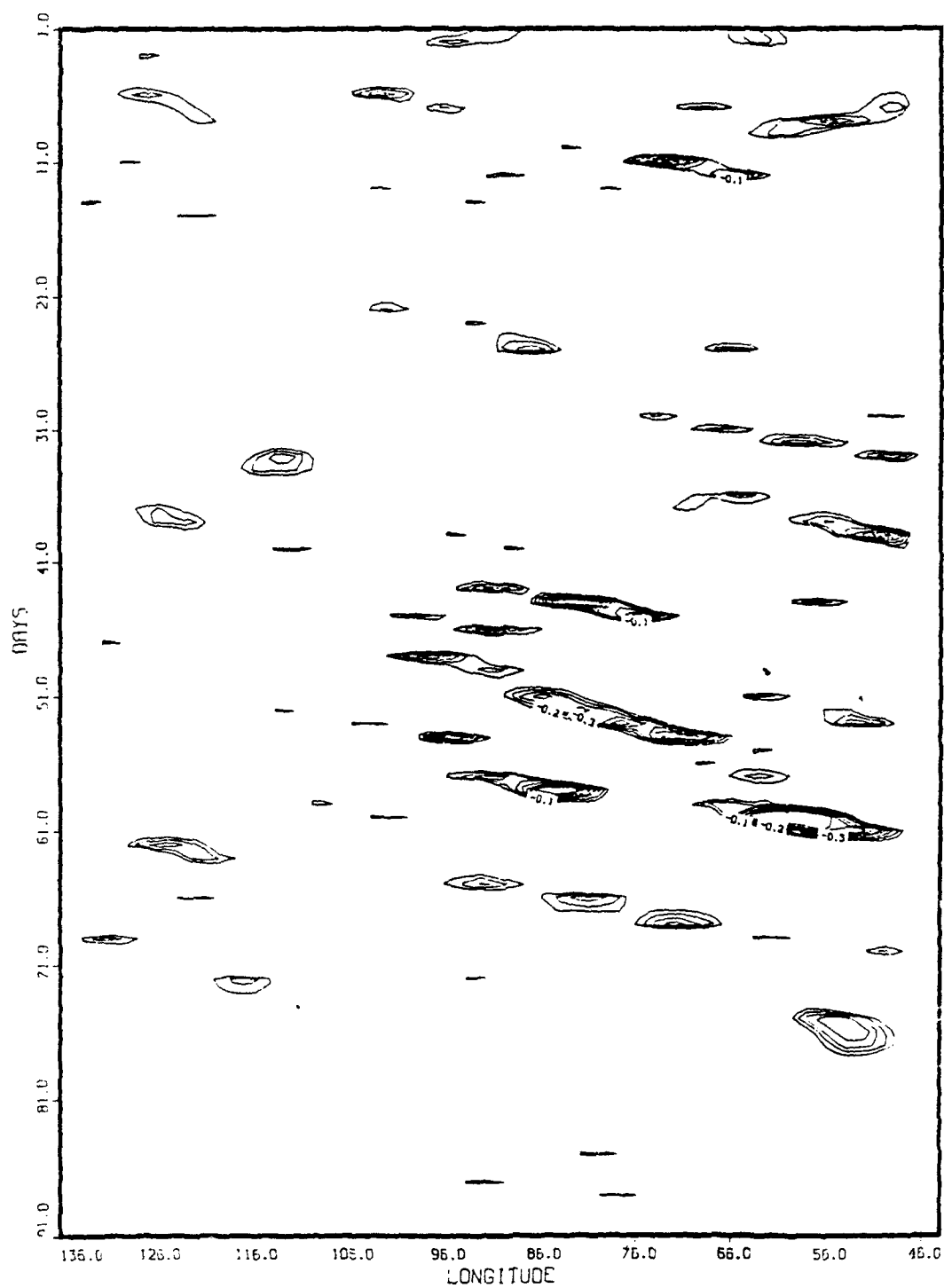


Figure 31. As in Fig. 25, except 33°N.

these events are local, shortlived, and do not propagate; at 9°N possible eastward propagation is occasionally noted. However, Figs. 28, 29, 30 and 31 still show a marked regularity for propagating negative temperatures. The limb effect apparently has meridional structure - its amplitude increases with increasing latitude up to 25°N through the tropics. It is generally not possible to design a single filter, independent of latitude, which will remove limb darkening, even across the limited tropical domain. This would imply that observational bias may still exist in the latitude-centered series, especially at latitudes north of 9°N . There seems to be some random character to this signal as well. Although the features still seem to be due to limb darkening, the existence of a synoptic wave cannot be ruled out absolutely.

CHAPTER VII

INTERACTIONS OF TROPICAL SYNOPTIC-SCALE FEATURES

With detection of the 12 d oscillation throughout the regime, the question arises concerning the existence of any interactions between this oscillation and other tropical synoptic-scale features.

To determine if there were any interactions between the 12 d oscillation and the 2800 km thermal wave, the gridded OLR data were filtered using the non-linear recursive band-pass filter described and used in Chapter V. The central wavelength of the filter in this study was 3000 km (full response) and the half amplitude points were 2200 km and 3300 km at the equator. The central wavelength and the half amplitude points were chosen to fit a 2800 km wave to the OLR gridded data between the equator and 20°N. The filter was applied to data centered on latitudes 0°, 3°, 10°, 13°, and 20°N for each day of the dry season. Hovmoller diagrams for the resulting filtered OLR at each of these latitudes are shown in Figs. 32-36. Only negative (cloudy) anomaly areas are shown in Figs. 32-36 for clarity.

The character of the time evolution of spatially filtered OLR varies with latitude. Near the equator (Figs. 32

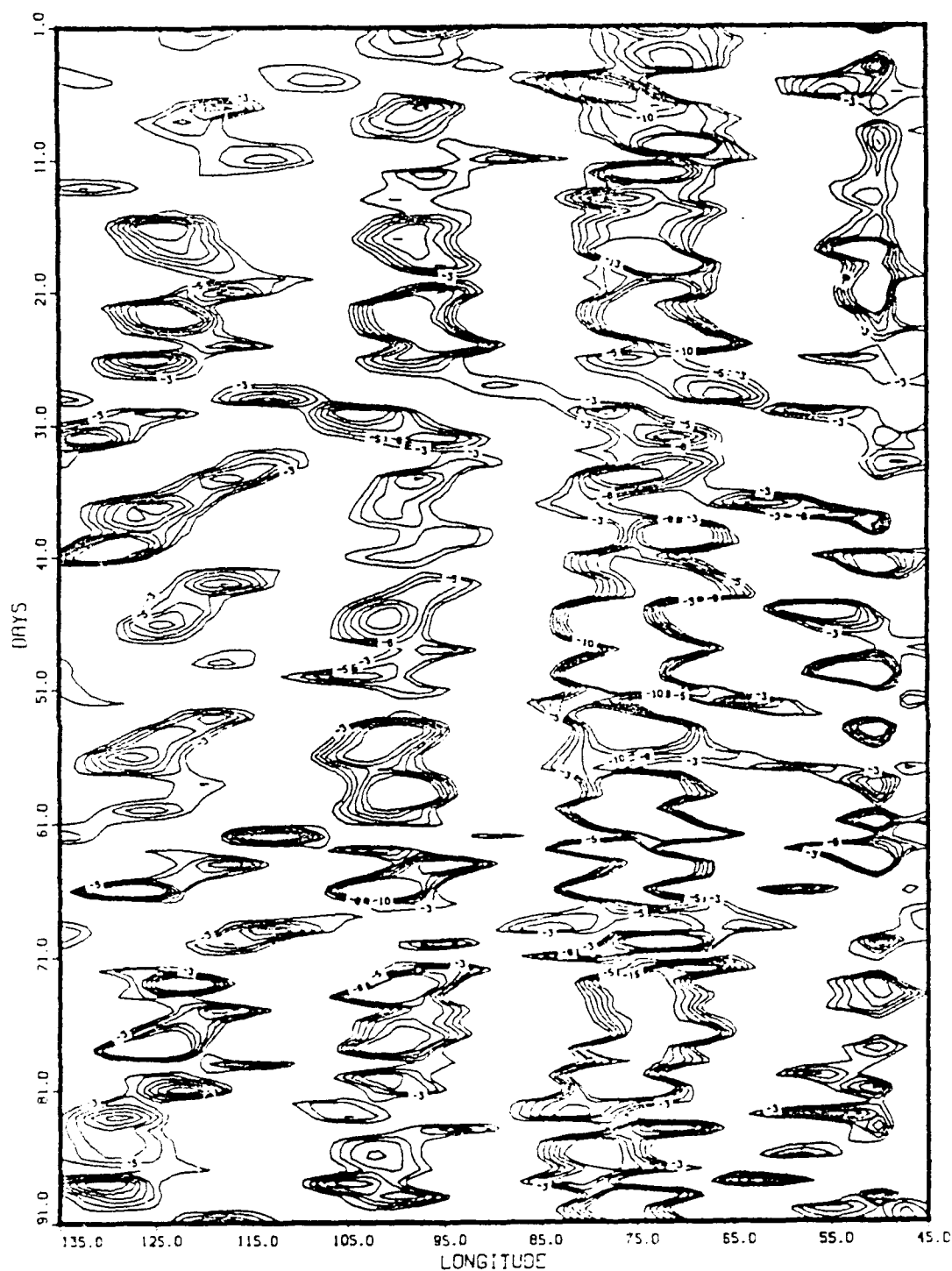


Figure 32. Results of filtering daily-averaged OLR gridded data (1 January - 9 May 1984) to fit a 2800 km wave, centered at the equator over 135°-45°W in Wm^{-2} .

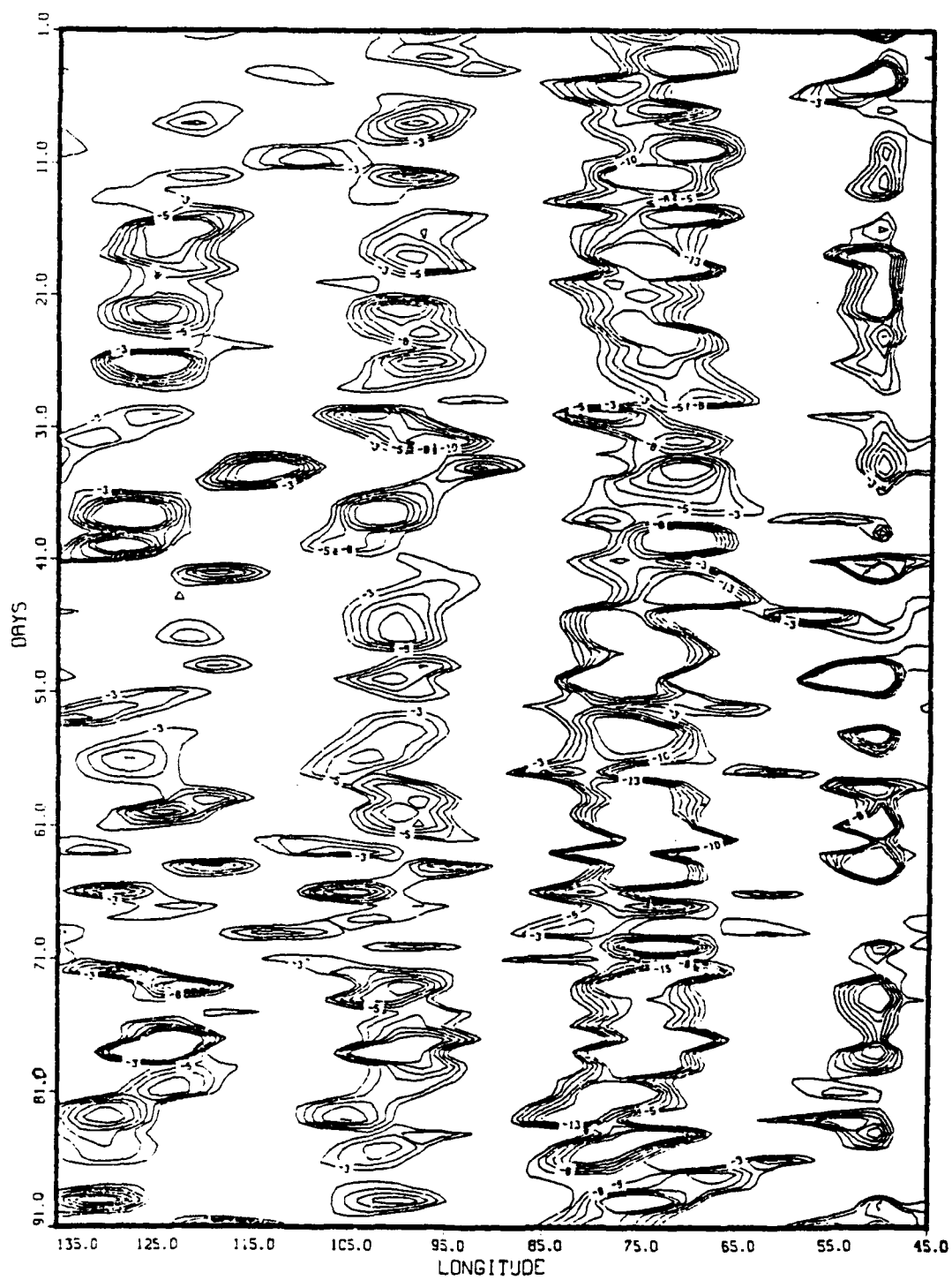


Figure 33. As in Fig. 32, except 3°N .

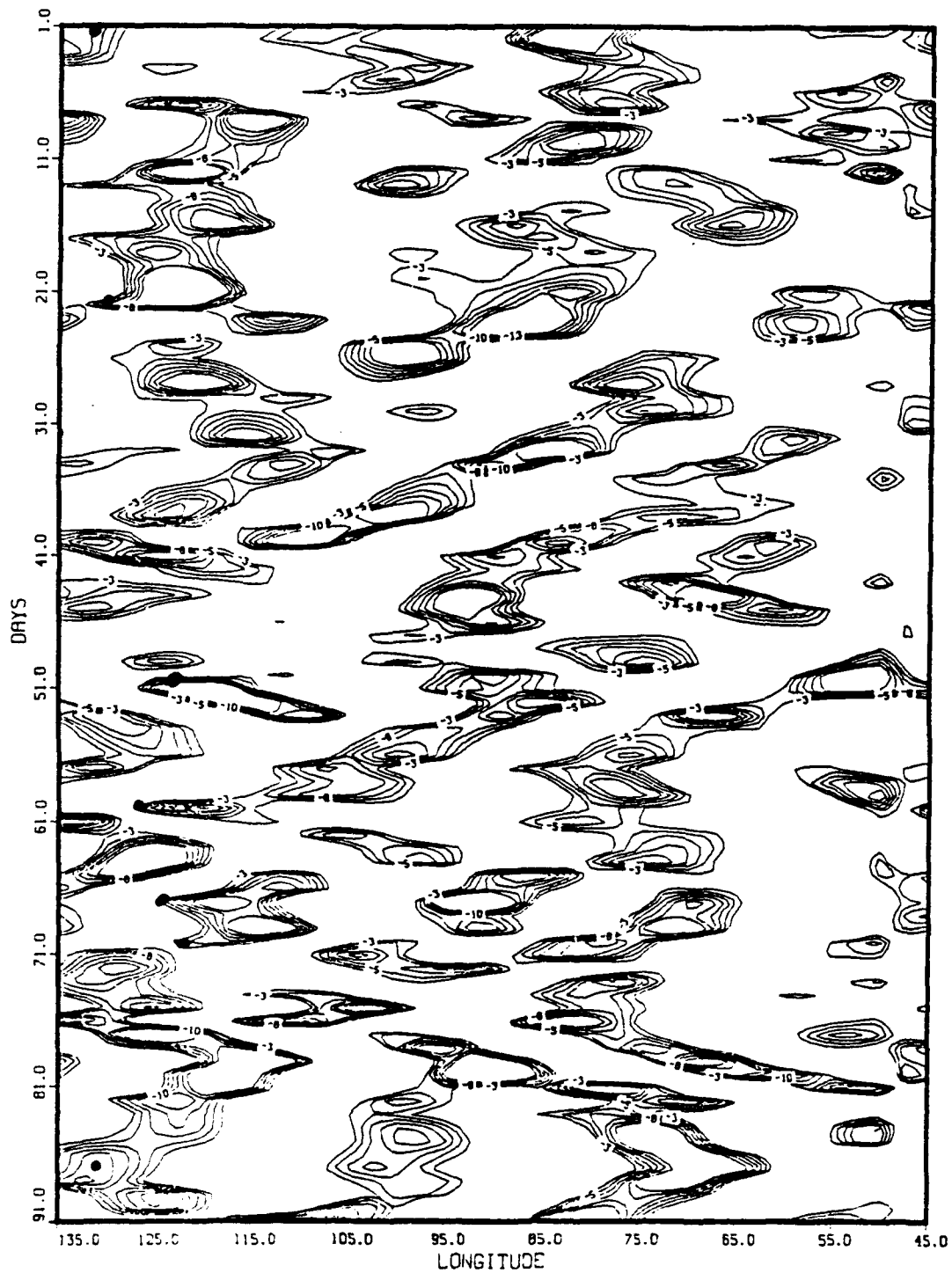


Figure 34. As in Fig. 32, except 10°N.

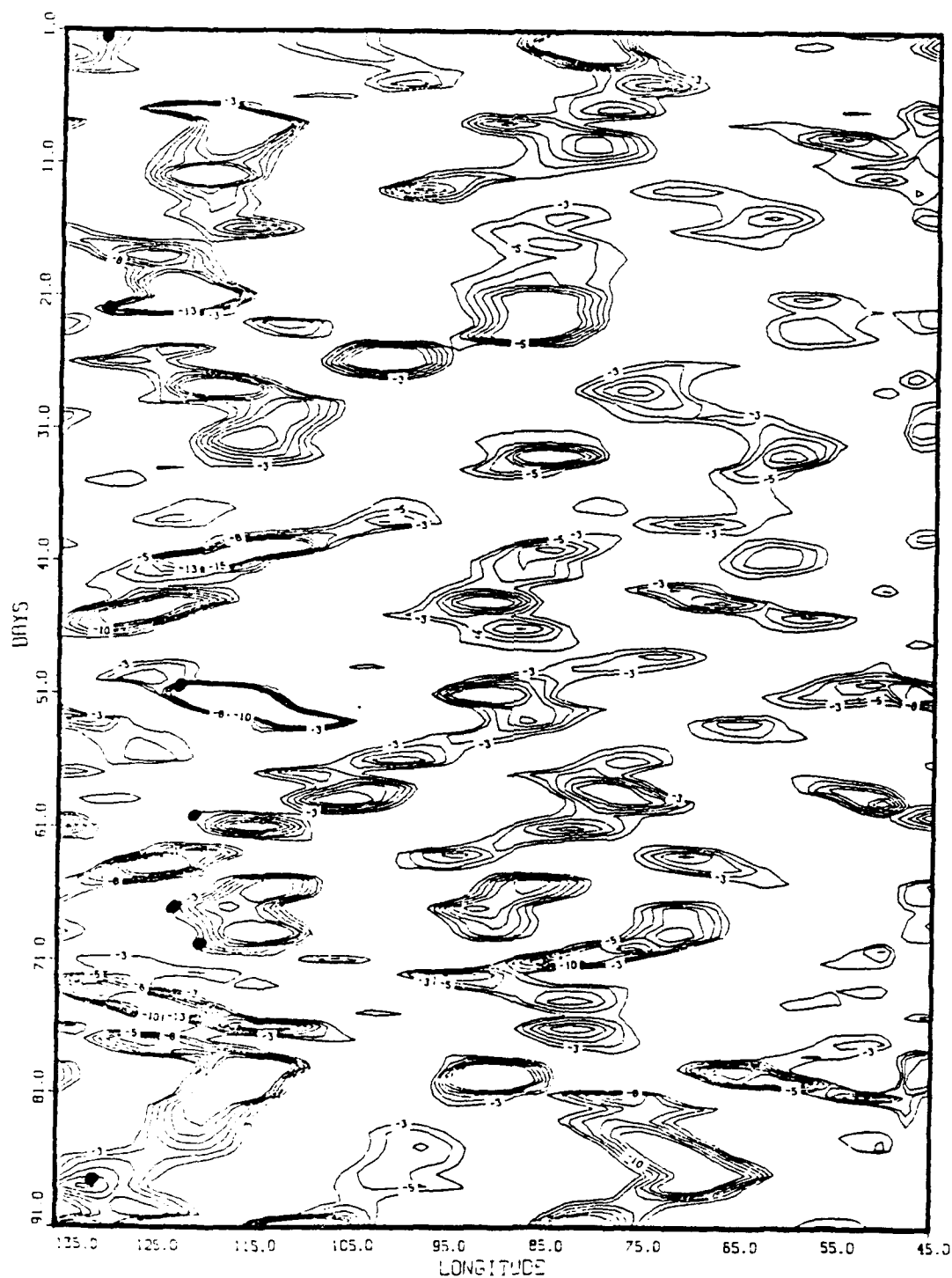


Figure 35. As in Fig. 32, except 13°N.

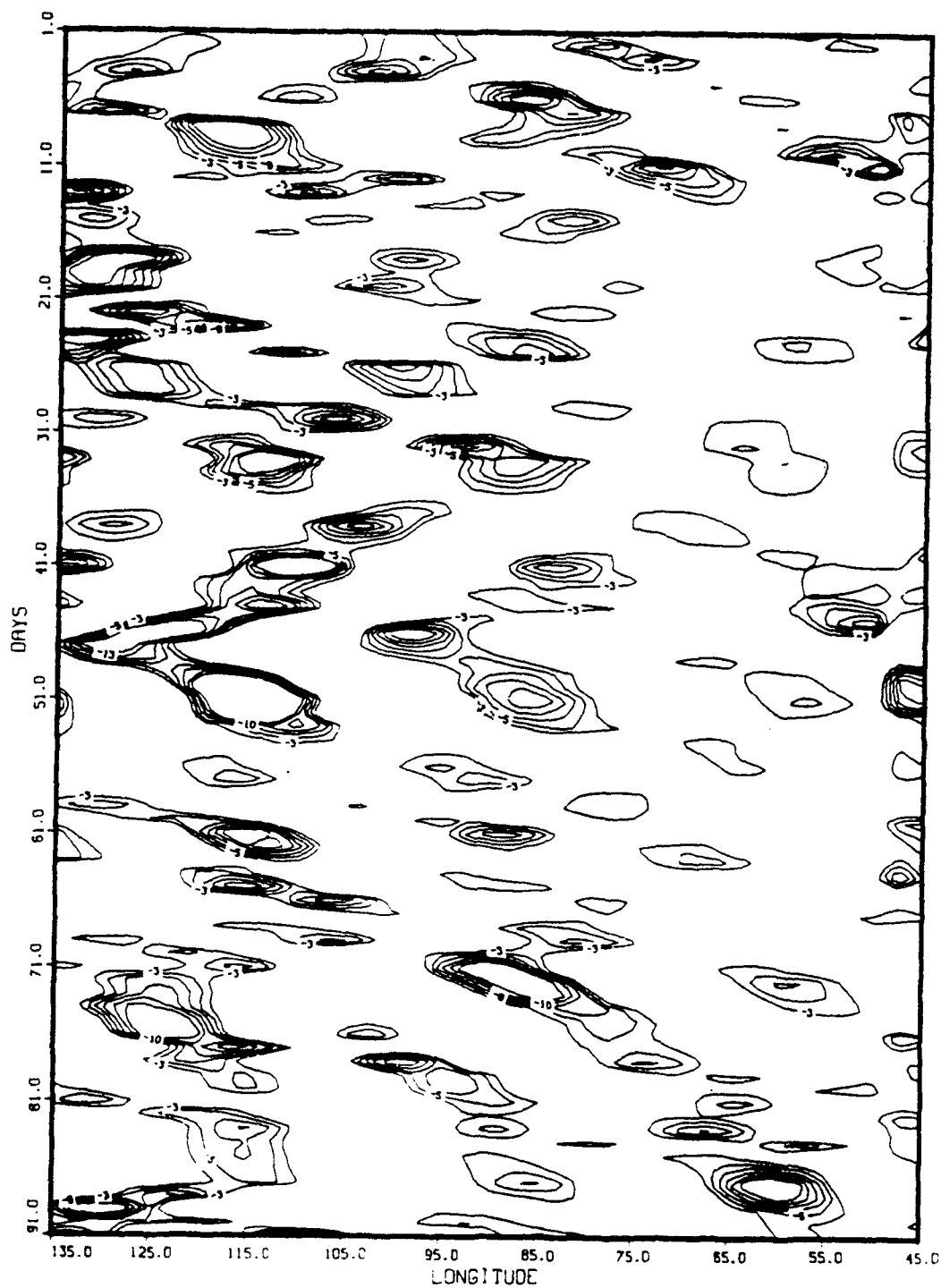


Figure 36. As in Fig. 32, except 20°N.

and 33), 3000 km waves tend to be stationary, particularly east of 120°W . A comparison between Figs. 20 and 34 reveal that there is little to no correspondence in the negative anomaly areas. Two implications are immediate: 1) The OLR observations are not contaminated by limb darkening; 2) TOVS temperature channels carry different signals than OLR window (cloud) observations. This comparison further illustrates the mistake of using the TOVS data to detect the 2800 km thermal wave in the upper troposphere. It is also important to note that a similar regularity and repetitiveness of an anomaly pattern as seen in the filtered TOVS data (Figs. 18-24) is not to be found in the filtered OLR data (Figs. 32-36). This is another indication that the OLR observations are not contaminated by limb darkening.

Significant features are apparent on the OLR Hovmoller diagrams. There is a standing wave apparent near the equator (Figs. 32 and 33) throughout the domain, with above average convection occurring at 125° , 100° , 75° , 50° , but strongest at 75°W . This wave disappears north of 3°N . This feature was also detected in OLR Hovmoller diagrams constructed for the corresponding latitudes in the Southern Hemisphere (not shown here). There is moderate propagation of the anomalies to the west, especially over the Pacific to the west of 110°W . The standing component is strongest and most persistent at about 80°W , which corresponds to the South American coastline and the foothills of the Andes. Therefore this standing wave

appears to be an effect of the Andes Mountains or of the Southern Hemisphere westerlies that are located along the west coast of the South American continent. Examination of daily satellite imagery suggests that persistent convection is a real meteorological phenomenon. In Figs. 34, 35, and 36 there are both westerly and easterly progressing OLR anomalies. The locations and dates of these anomalies were compared with infrared (IR) satellite imagery. The anomalies could be readily identified in the imagery as the cloudy areas associated with convection. Propagation over the ocean is most persistent. The Central American coastline is at about 85°W at 10°N and at 105°W at 20°N . At 20°N (Fig. 36), anomalies and propagation are weak to the east of Yucatan (east of 85°W). At this latitude eastward propagation dominates, except for the one strong episode which commences over Yucatan and moves to the west between days 30 and 50. At individual longitudes, the separation between convective episodes appears to occur within the 12 d band, again restricted to regions west of Yucatan.

Deeper in the tropics, at 10° and 13°N (Figs. 34 and 35) westward propagation is strong, particularly up to about day 60. Many convective episodes, both eastward and westward propagating, can be tracked for periods over two weeks. At 10°N eastward and westward propagation appears to occur simultaneously, with constructive and destructive interferences leading to isolated convective maxima of 2-3 d duration.

Convective episodes seem to occur at intervals of 8-12 d. There is a tendency for convective episodes to be stronger over Central American topography and coastlines, leading to a standing component of filtered OLR, although this feature is not as strong as the standing component at 3°N .

As previously discussed in Chapter V, the 12 d oscillation is most apparent over the east Pacific basin and Central America. McGuirk et al (1987) found that few tropical plume events occur east of 110°W . Tables 1 and 3 which give origin times and locations for some tropical plumes, were used to plot the locations on Figs. 34 and 35 (locations are denoted with a dark circle). The evolution of the tropical plumes' cloud shields can be followed through time in Figs. 34 and 35 by following the eastward progression of the negative anomalies that relate to the cloud shields. Although most of the plume origins seem to fall on westward propagating convective maxima, there is no clear relationship between convection in the 3000 km band and tropical plumes. The majority of the convective episode occur in the 3000 km - 2 to 12 d band and do not resemble tropical plumes.

Finally, Knutson and Weickmann (1987) described a 30-60 d oscillation in the velocity potential at 250 mb and enhanced convection of the tropics. To see if there is any interaction between this oscillation and the 12 d oscillation, a Hovmoller diagram of the filtered OLR data for the year 1984 and averaged over 5°N - 5°S was constructed (Fig. 37).

Convective episodes seem to occur at intervals of 8-12 d. There is a tendency for convective episodes to be stronger over Central American topography and coastlines, leading to a standing component of filtered OLR, although this feature is not as strong as the standing component at 3°N .

As previously discussed in Chapter V, the 12 d oscillation is most apparent over the east Pacific basin and Central America. McGuirk et al (1987) found that few tropical plume events occur east of 110°W . Tables 1 and 3 which give origin times and locations for some tropical plumes, were used to plot the locations on Figs. 34 and 35 (locations are denoted with a dark circle). The evolution of the tropical plumes' cloud shields can be followed through time in Figs. 34 and 35 by following the eastward progression of the negative anomalies that relate to the cloud shields. Although most of the plume origins seem to fall on westward propagating convective maxima, there is no clear relationship between convection in the 3000 km band and tropical plumes. The majority of the convective episode occur in the 3000 km - 2 to 12 d band and do not resemble tropical plumes.

Finally, Knutson and Weickmann (1987) described a 30-60 d oscillation in the velocity potential at 250 mb and enhanced convection of the tropics. To see if there is any interaction between this oscillation and the 12 d oscillation, a Hovmoller diagram of the filtered OLR data for the year 1984 and averaged over 5°N - 5°S was constructed (Fig. 37).

Table 3. List of tropical plumes for March 1984. Provided by J. G. Lee (Texas A&M Univ.).

<u>March 1984</u>			
Case	Start	Dissipation	Origin Long
A	00 UTC 3	00 UTC 5	128°W
B	12 UTC 5	00 UTC 7	115°W
C	12 UTC 7	00 UTC 9	125°W
D	12 UTC 15	12 UTC 17	135°W
E	00 UTC 19	00 UTC 22	145°W
F	00 UTC 25	12 UTC 27	140°W

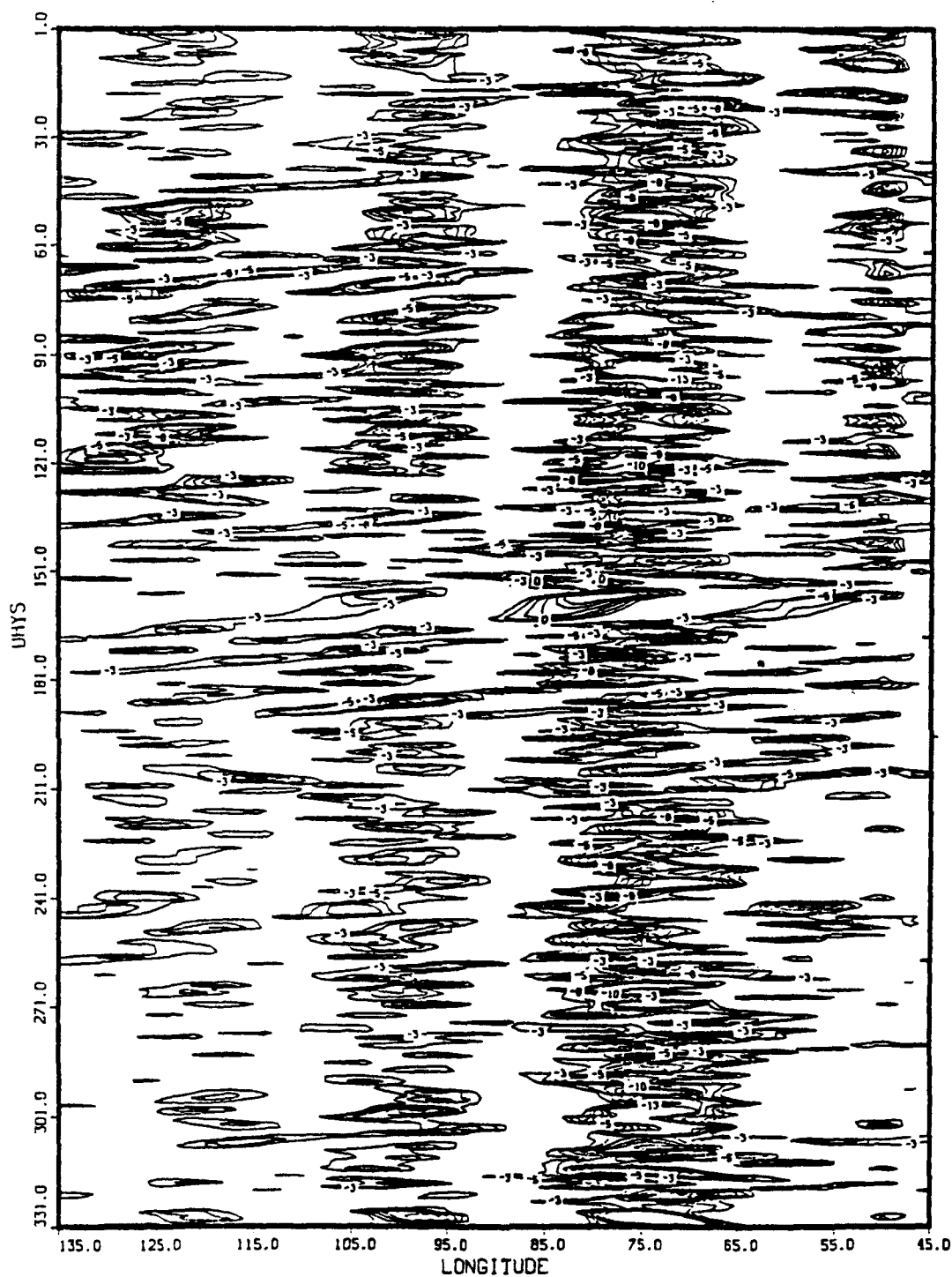


Figure 37. Results of filtering daily-averaged OLR gridded data (1 January - 4 December 1984) to fit a 2800 km wave, averaged and centered at 5°N-5°S over 135°-45°W in Wm^{-2} .

Also shown in Fig. 37 is the passage of velocity potential minima associated with the 30-60 d wave. Apparent in Fig. 37 is the standing convective regions at 75° and 100°W . Westward propagation is seen in many convection peaks. Negative velocity potential is indicative of upper level divergence (250mb). In terms of the filtered OLR data in Fig. 37, negative (cloudy) anomaly areas would be expected to be present when there is negative velocity potential anomalies. In other words, there would be an oscillation in the negative anomaly areas of 30-60 days. An examination of Fig. 37 suggest that there is a slight indication of this occurring at 135° - 95°W . An example can be seen beginning around day 65 at 130°W . There is a period of convection followed by a decrease to no convection as one progresses eastward (in time) to around 110°W . Again, proceeding eastward (in time), convection begins and reaches a maxima around day 100 at 100°W . However, the change from the dry to the wet season (at day 130) can be easily identified in the anomaly patterns over the Pacific Ocean (135° - 95°W) in Fig. 37. During wet season, the interaction is difficult to find in that area. The beginning just west of South America (90° - 65°W) shows ver little correlation with the 30-60d wave.

CHAPTER VIII

SUMMARY AND DISCUSSION

Convective variability over the east Pacific basin was examined through spectral analysis of OLR time series. In the dry season, spectral peaks were located at near 52 d, 24 d and 13 d. The largest peaks appeared at around 7 d and 5 d. The wet season analysis showed peaks at around the same days except the peak near 50 d was missing. The peak near 7 d was found to be not physically relevant. The 5 d peak has been noted by others and was not considered further in this study. The OLR time series for the dry and wet seasons were filtered for 12 d oscillations and composite diagrams corresponding to each of the four phases (Maximum, Minimum, and two inflection points) of this oscillation were constructed for the eastern Pacific/Central American domain (140° - 40° W and 35° N- 35° S). The following conclusions were drawn from the composite analyses:

- The composites for dry season revealed a preferred meridional (north-south) orientation of OLR anomalies with a consistent eastward movement. The strength of the anomalies ranged from -9.0 to +9.0 Wm^{-2} .

- The composites for wet season differ from dry season in that the OLR anomalies have a different directional movement (westward). The strength of the anomalies is similar to those in dry season.

The existence of a 2800 km thermal wave in the upper troposphere was called into question through the use of non-linear filtering and regression of TOVS HIRS-2 Channel 3 brightness temperatures. The signal for the thermal wave in this channel appears to be a result of satellite limb brightening/darkening that has not been corrected properly. However, some signals, both in HIRS radiances and in spatially filtered OLR suggest that meteorological behavior in the 12 d band exists at some times and places.

Interactions between the 12 d oscillation and tropical plumes were detected. Areas of negative OLR anomalies in Hovmoller diagrams correspond to the origin times and locations of previously identified tropical plumes. Evolution of the cloud shields could be followed. Often, but not always, westward propagating convective maxima evolved into tropical plumes. Many convective episodes, even those existing on 12 d time scales and 2800 km space scales, are not related to tropical plumes.

Perhaps the two most significant findings in this work are phenomena which appear in meteorological data sets, but owe their origin to non-meteorological causes: 1) The

description of a 2800 km thermal wave by Schaefer (1988) in TOVS multi-channel data is largely illusionary. It results from systematic limb darkening effects which survived several computations procedures designed to remove them. Thus, while it cannot be concluded that behavior at 2800 km wavelengths is not important in tropical systems, the apparent abiogenesis described by Schaefer (1988) is incorrect. 2) A spike in area-averaged OLR gridded data occurs every 7 days. This fluctuation has not been described before, but it appears strongly in regional temporal spectra. It is marked by warmer than believable OLR minima in convectively active regions, particularly over the Amazon Basin. Although the cause of this 7 d spike was not determined, it certainly is not meteorological.

Possible connections between the 12 d oscillation and the 30-60 oscillation was examined. The limited time series of this study prohibits firm conclusions being drawn, but obvious connections are absent.

Besides the progress described above, this study has raised several other relevant lines of work:

- Examine several years of OLR data to determine the interannual variability of the 12 d oscillation.
- Expand the domain of the OLR data to see if this 12 d oscillation encircles the globe.

- Examine several years of global OLR data to determine the extent of the 7 d spike that appeared in the unfiltered OLR time series of this study.
- Analyze other years of space and time filtered OLR data to see if there are similar results in Hovmoller diagrams (e.g., the existence of the standing and the propagating waves).
- Correct the satellite limb brightening/darkening effect systematically. After the correction, search the TOVS data for residual existence of a meteorologically significant thermal wave.
- Resolve important scale interactions (12 d wave, 2800 km wave, tropical plumes, 30-60d wave) over many years of observations.

REFERENCES

- Anderson, L. L., Jr., 1986: *Multispectral analysis of a tropical radiance set from TIROS operational vertical sounder*. Ph.D. Dissertation, Dept. of Meteorology, Texas A&M University, 229 pp.
- Atkinson, G. D., 1971: *Forecasters' guide to tropical meteorology*. AWS Technical Report 240, St. Louis, 360 pp.
- Barnes, S. L., 1964: A technique for maximizing details in numerical weather map analysis. *J. Appl. Meteor.*, 3, 396-409.
- Dunn, G. E., 1940: Cyclogenesis in the tropical Atlantic. *Bull. Amer. Meteor. Soc.*, 6, 133-146.
- Gruber, A., and C. D. Watkins, 1982: Statistical assessment of the quality of TIROS-N and NOAA-6 satellite soundings. *Mon. Wea. Rev.*, 110, 867-876.
- , and J. S. Winston, 1978: Earth-atmosphere radiative heating based on radiometer measurements. *Bull. Amer. Meteor. Soc.*, 59, 1570-1573.
- Hastenrath, S., 1988: *Climate and Circulation of the Tropics*. D. Reidel Publishing Co., Dordrecht, 455 pp.
- International Mathematical and Statistical Library User's Manual*, The IMSL Inc., Houston, 1987.

- Knutson, T. R., and K. M. Weickmann, 1987: 30-60 day atmospheric oscillations: Composite life cycles of convection and circulation anomalies. *Mon. Wea. Rev.*, 115, 1407-1436.
- , -----, and J. E. Kutzbach, 1986: Global-scale interseasonal oscillations of outgoing longwave radiation and 250 mb zonal wind during northern hemisphere summer. *Mon. Wea. Rev.*, 114, 605-623.
- Lau, K. -M., and N. C. Lau, 1990: Observed structure and propagation characteristics of tropical summertime synoptic scale disturbances. *Mon. Wea. Rev.*, 118, 1888-1913.
- , Li Peng, C. H. Sui, and T. Nakazawa, 1989: Dynamics of super cloud clusters, westerly wind bursts, 30-60 day oscillation and ENSO: An unified view. *J. Meteorol. Soc. Jpn.*, 67, 205-219.
- , and P. H. Chan, 1983: Aspects of the 40-50 day oscillation during the northern summer as inferred from outgoing longwave radiation. *Mon. Wea. Rev.*, 114, 1354-1367.
- Liebmann, B., and H. H. Hendon, 1990: Synoptic-scale disturbances near the equator. *J. Atmos. Sci.*, 47, 1463-1479.
- Lyons, S. W., 1981: Planetary-scale aspects of outgoing longwave radiation and vorticity over the global tropics during winter. *Mon. Wea. Rev.*, 109, 1773-1787.

- Madden, R. A., and P. R. Julian, 1972: Description of a global-scale circulation cells in the tropics with a 40-50 day period. *J. Atmos. Sci.*, 29, 1109-1123.
- , and -----, 1971: Detection of a 40-60 day oscillation in the zonal wind in the tropical Pacific. *J. Atmos. Sci.*, 28, 702-708.
- McGuirk, J. P., and D. J. Ulsh, 1990: Evolution of tropical plumes in VAS water vapor imagery. *Mon. Wea. Rev.*, 118, 1758-1766.
- , A. H. Thompson, and N. R. Smith, 1987: Moisture bursts over the tropical Pacific Ocean. *Mon. Wea. Rev.*, 115, 787-798.
- Merritt, E. S., 1964: Easterly waves and perturbations, a reappraisal. *J. Atmos. Sci.*, 3, 367-382.
- Murakami, T., 1980: Empirical orthogonal function analysis of satellite-observed outgoing longwave radiation during winter. Part I. Long-period (15-30 day) oscillations. *Mon. Wea. Rev.*, 108, 408-426.
- Panofsky, H. A., and G. W. Brier, 1968: *Some Applications of Statistics to Meteorology*, The Pennsylvania State University, University Park, 224 pp.
- Riehl, H., 1954: *Tropical Meteorology*. McGraw-Hill, New York, 392 pp.
- , 1945: Waves in the easterlies and the polar front in the tropics. Dept. of Meteorology, University of Chicago, Misc. Rept. 17, Chicago, 79 pp.

- Sadler, J. C., 1967: On the origin of tropical vortices. Proc. of the Working Panel on Tropical Dynamic Meteorology, NWRP 12-1167-132, Navy Weather Research Facility, Monterey, 39-76.
- Schaefer, J. R., 1988: *Synoptic scale tropical waves in multichannel satellite radiance data*. Ph.D. Dissertation, Dept. of Meteorology, Texas A&M University, 117 pp.
- Shanks, J. L., 1967: Recursion filters for digital processing. *Geophysics*, 32, 33-51.
- Smith, W. L., H. M. Woolf, C. M. Hayden, D. Q. Wark, and L. M. McMillin, 1979: The TIROS-N operational vertical sounder. *Bull. Amer. Meteor. Soc.*, 58, 1177-1187.
- , and -----, 1976: The use of eigenvectors of statistical covariance matrices for interpreting satellite sounding radiometer observations. *J. Atmos. Sci.*, 33, 1127-1140.
- Strager, C. S., 1989: *Origins of convective activity over Panama*. M.S. Thesis, Dept. of Meteorology, Texas A&M University, 112 pp.
- Ulsh, D. J., 1988: *Moisture burst structure in satellite water vapor imagery*. M.S. Thesis, Dept. of Meteorology, Texas A&M University, 101 pp.
- Wallace, J. M., and C. -P. Chang, 1969: Spectrum analysis of large-scale wave disturbances in the tropical lower troposphere. *J. Atmos. Sci.*, 26, 1010-1025.

Weickmann, K. L., G. R. Lusk, and J. E. Kutzbach, 1985:

Interseasonal (30-60 day) fluctuation of outgoing longwave radiation and 250 mb streamfunction during northern winter. *Mon. Wea. Rev.*, 113, 941-961.

-----, 1983: Interseasonal circulation and outgoing longwave radiation modes during northern hemisphere winter. *Mon. Wea. Rev.*, 111, 1838-1858.

Yasunari, T., 1980: A quasi-stationary appearance of 30-40 day period in the cloudiness fluctuations during the summer monsoon over India. *J. Meteor. Soc. Jpn.*, 58, 225-229.

VITA

Susan Elizabeth Winton was born on December 7, 1957 in Elyria, Ohio to Ernest and Elizabeth Janik. Susan completed her secondary education at Elyria Catholic High School in June 1975. She enlisted in the US Army and served as a finance specialist at Fort Stewart, Georgia and Fort Shafter, Hawaii. In 1981, Susan attended Gannon University in Erie, Pennsylvania. She was awarded a Bachelor of Science degree in Mathematics (1984).

Upon graduation from Officer Training School at Lackland AFB, Texas (1984), Susan attended the Basic Meteorology program at Texas A&M University. She served as the Wing Weather Officer to the 7th Bomb Wing at Carswell AFB, Texas from June 1986 through October 1987. Her next assignment was in Panama at Howard AFB. Susan was the Meteorological Satellite Coordinator and Staff Weather Officer the US Air Force Southern Air Division. While in Panama, she was selected to pursue her Masters degree in Meteorology by the Air Force Institute of Technology. Susan began her studies at Texas A&M University in June of 1989.

She is the proud mother of Joylyn Catherine Winton. Susan's permanent address is: 344 Griswold Road, Elyria, Ohio 44035.